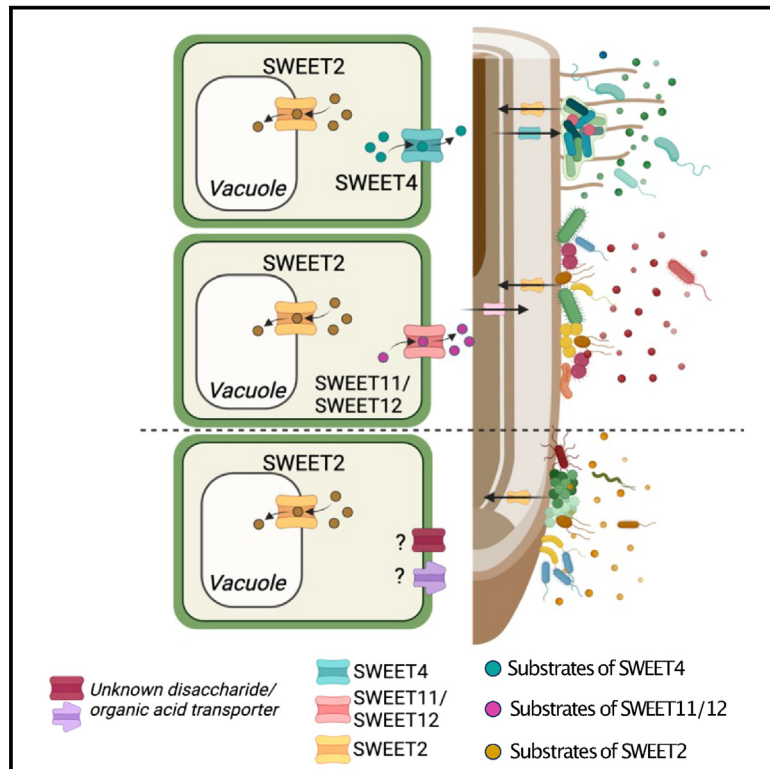


Cell Host & Microbe

Sugar transporters spatially organize microbiota colonization along the longitudinal root axis of *Arabidopsis*

Graphical abstract



Authors

Eliza P.-I. Loo, Paloma Durán, Tin Yau Pang, ..., Martin Lercher, Ruben Garrido-Oter, Wolf B. Frommer

Correspondence

loo@hhu.de (E.P.-I.L.),
frommew@hhu.de (W.B.F.)

In brief

Loo et al. develop two growth systems to define the spatial organization of microbiota and metabolites along the longitudinal axis of the *Arabidopsis thaliana* root. SWEET sugar transporters contribute to the distribution of sugar (and other metabolites) along the root, which is required for spatial colonization of root bacteria.

Highlights

- Root microbiota, metabolites, and SWEET uniporters are patterned along the root axis
- SWEET sugar uniporter organization correlates with sugar metabolism pathways in the root
- Root metabolites and microbiota are spatially reorganized in *sweet*-deficient plants
- SWEET2, -4, and -11;12 play a functional role in spatial colonization of microbiota



Article

Sugar transporters spatially organize microbiota colonization along the longitudinal root axis of *Arabidopsis*

Eliza P.-I. Loo,^{1,6,9,11,*} Paloma Durán,^{2,6,9,10} Tin Yau Pang,^{3,5} Philipp Westhoff,^{4,6} Chen Deng,¹ Carlos Durán,² Martin Lercher,^{3,5} Ruben Garrido-Oter,^{2,6,7} and Wolf B. Frommer^{1,6,8,*}

¹Heinrich Heine University Düsseldorf, Faculty of Mathematics and Natural Sciences, Institute for Molecular Physiology, 40225 Düsseldorf, Germany

²Department of Plant-Microbe Interactions, Max Planck Institute for Plant Breeding Research, 50829 Cologne, Germany

³Heinrich Heine University Düsseldorf, Faculty of Mathematics and Natural Sciences, Institute for Computer Science and Department of Biology, 40225 Düsseldorf, Germany

⁴Heinrich Heine University Düsseldorf, Faculty of Mathematics and Natural Sciences, Plant Metabolism and Metabolomics Laboratory, 40225 Düsseldorf, Germany

⁵Heinrich Heine University Düsseldorf, Medical Faculty and University Hospital Düsseldorf, Division of Cardiology, Pulmonology and Vascular Medicine, 40225 Düsseldorf, Germany

⁶Cluster of Excellence on Plant Sciences, 40225 Düsseldorf, Germany

⁷Earlham Institute, Norwich NR4 7UZ, UK

⁸Institute of Transformative Bio-Molecules (WPI-ITbM), Nagoya University, 464-8601 Nagoya, Japan

⁹These authors contributed equally

¹⁰Present address: Laboratoire des Interactions Plantes-Microbes-Environnement, Institut National de Recherche pour l'Agriculture, l'Alimentation et l'Environnement, CNRS, Université de Toulouse, 31320 Castanet-Tolosan, France

¹¹Lead contact

*Correspondence: loo@hhu.de (E.P.-I.L.), frommer@hhu.de (W.B.F.)

<https://doi.org/10.1016/j.chom.2024.02.014>

SUMMARY

Plant roots are functionally heterogeneous in cellular architecture, transcriptome profile, metabolic state, and microbial immunity. We hypothesized that axial differentiation may also impact spatial colonization by root microbiota along the root axis. We developed two growth systems, ArtSoil and CD-Rhizotron, to grow and then dissect *Arabidopsis thaliana* roots into three segments. We demonstrate that distinct endospheric and rhizosphere bacterial communities colonize the segments, supporting the hypothesis of microbiota differentiation along the axis. Root metabolite profiling of each segment reveals differential metabolite enrichment and specificity. Bioinformatic analyses and GUS histochemistry indicate microbe-induced accumulation of SWEET2, 4, and 12 sugar uniporters. Profiling of root segments from *sweet* mutants shows altered spatial metabolic profiles and reorganization of endospheric root microbiota. This work reveals the interdependency between root metabolites and microbial colonization and the contribution of SWEETs to spatial diversity and stability of microbial ecosystem.

INTRODUCTION

In human and other model animal systems, the gut microbiota is differentially distributed along both the longitudinal and transverse axes due to physiological variations, including nutrient and chemical gradients, intestinal architecture, and host immunity.^{1–3} The midgut of *Drosophila* consists of subregions, where cells in subregions perform specific functions and have different immune responses.⁴ Accordingly, the host senses and balances the populations of harmful and beneficial microbes across the different regions in the gut.⁵

Similar to the guts of animals, plants have evolved specialized organs, i.e., roots, for nutrient acquisition.^{6,7} Roots also harbor

specific bacterial communities that extend the host's metabolic repertoire.⁸ The core principles of microbiota establishment within the gut and plant roots are similarly driven by nutrition, host genotype, immune system, and microbe-microbe interactions.^{6,9,10} Since the root shows functional heterogeneity at the levels of cell differentiation, transcriptome, metabolic states, and immune responses,^{11–16} it is likely that the variability of these factors in the root gives rise to regionalization of the root microbiota. However, current literature lacks information^{17,18} on spatial differentiation and its drivers, which could help to better understand the colonization strategies of root-associated microbes.

Plant roots are responsible for water and nutrient uptake from the soil, and roots release up to 20% of the photosynthetically



fixed carbon into the soil via rhizodeposition through processes such as root exudation.^{19,20} Since the late 1950s, researchers have reported active exudation sites in the root and shown that different compounds are released from different parts of the root.²¹ Recent metabolite mapping of root cells showed differences in levels and localization of metabolites in different cell types.¹⁵ A recent metabolite atlas for *Medicago* root tissues revealed a differential accumulation of metabolites between root cell types.²² Extensive studies have been performed to compare metabolic changes within the root as a result of biotic and/or abiotic stimuli that alter the composition of root exudates. It is well established that the metabolite composition of the root exudate affects root microbiota.^{23–25} However, it remains to be investigated whether and how the spatial distribution of metabolites in the root affects spatial colonization by root microbiota.

Among the numerous components exuded from roots, the three most abundant classes of organic substances with low molecular weight are sugars, carboxylic acids, and amino acids.¹⁹ It remains unclear why plants invest high amounts of photosynthetically fixed carbon into root exudates. The rates of monosaccharide uptake by microorganisms range from seconds to minutes,²⁶ rendering sugar uptake by soil microbes a strong sugar sink in the soil. Hence, ecological theories pose that root exudation is a mechanism plants acquired for survival advantages via the recruitment of beneficial microorganisms for the provision of other essential nutrients or for strengthening immune responses.²⁷

SWEETs are sugar uniporters found in many pro- and most eukaryotes.²⁸ SWEETs transport monosaccharides and/or disaccharides along the substrate concentration gradient. Most diploid plant genomes contain about 20 SWEET genes.²⁹ SWEETs play important roles across multiple plant species in various physiological processes, including phloem loading and unloading, seed filling, pollen nutrition, and nectar secretion. SWEETs have also been implicated in several symbiotic interactions, including those of arbuscular mycorrhizal fungi with potato, soybean, and *Medicago*, and between nitrogen-fixing rhizobia and lotus.^{30–33} In *Arabidopsis thaliana* (*A. thaliana*), there are 17 SWEET uniporter homologs, classified as AtSWEET1 to AtSWEET17 into 4 clades, whereby clade I members (SWEET1–SWEET3) mainly transport hexoses, clade II transporters (SWEET4–SWEET8) preferentially transport glucose, clade III members (SWEET9–SWEET15) mainly utilize sucrose as a substrate, and members of the clade IV (SWEET16 and SWEET17) mediate fructose transport.

There is evidence for the manipulation of SWEET transporter transcript abundance by pathogens and an impact of SWEET activities on virulence.²⁸ For instance, *sweet2* knock-out lines showed increased susceptibility to a pathogenic oomycete, intimating a role for AtSWEET2 in sequestering glucose into the vacuole to limit pathogen feeding.³⁴ Similarly, in rice, cassava, and cotton, *Xanthomonas* species hijack SWEET transporter activity, which is crucial for the growth and proliferation of the pathogens, since the inability to induce SWEETs results in disease resistance.^{35–38} Root-secreted sucrose triggers the synthesis of levans in the soil by the bacterium *Bacillus subtilis*, which in turn promotes solid-surface motility and root colonization.³⁹ Collectively, these studies intimate that microbes have built-in mechanisms for manipulating SWEETs for sugar efflux to facilitate colo-

nization and growth. Beyond plant-microbe mono-association studies,³⁴ SWEETs had not been demonstrated to play a role in plant-root microbiota interactions, i.e., a possibility for SWEETs to serve as a directory for root microbes to facilitate their proliferation along the root axis.

Here, we developed two plant growth systems to enable the dissection of roots into 2-cm segments for spatial microbiota and metabolite profiling. Amplicon sequencing revealed distinctive community structures along the length of the root that correlated with differences in metabolic profiles of the adjacent root segments. Since sugars play a more prominent role compared with organic acids in bacterial community assembly,^{40,41} we used public transcriptome repositories and bioinformatics to examine potential spatial differentiation of candidate sugar efflux transporter (SWEET) accumulation along the longitudinal root axis. *In silico* and histochemical analyses supported spatial divergence of accumulation of SWEET2, SWEET4, and SWEET12 sugar transporters along the root in a root microbe-dependent manner. Microbiota and metabolite profiling along the root segments of *sweet2*, *sweet4*, and *sweet11;12* knock-out lines provided evidence for the loss of spatial organization of both root microbiota and various metabolites. This work illustrates the involvement of SWEETs in maintaining the spatial distribution of the root microbial communities.

RESULTS

Development of CD-Rhizotron and artificial soil (ArtSoil) for testing differential microbiota colonization along the longitudinal root axis

We hypothesized that spatial differentiation of the root transcriptome¹¹ could lead to differential local bacterial colonization. To test this hypothesis, a growth system based on CD cases, which we named CD-Rhizotron, was developed to enable the dissection of individual root strands of plants grown in soil into segments (Figures 1A and S1A–S1E). To evaluate the microbiota community of roots grown in the CD-Rhizotron, full-length roots of *A. thaliana* grown in the CD-Rhizotron were compared with data from soil-grown plants that had previously been reported.^{42,43} Alpha and beta-diversities of the root microbiota were consistent with the root microbiota community observed in soil-grown plants (Figures S1F and S1G), validating the reliability of the CD-Rhizotron system to simulate soil growth conditions. Distinct clustering of 16S rRNA amplicon samples along the x-axis of the constrained principal coordinates analysis (CPCoA) using Bray-Curtis dissimilarities indicated that rhizospheric and endospheric root communities derived from the full-length root were significantly different from bulk soil, i.e., soil without plant growth. Further, decreased microbial alpha diversity was observed between the soil and the root endophytic compartments (Kruskal-Wallis, Dunn's test post hoc, $p = 0.001$; Figures S1F and S1G). The relative microbial abundances and alpha diversity of the soil and the rhizospheric and endospheric microbiota successfully reproduced phylum-level plant-enrichment patterns seen in soil-grown *A. thaliana*^{42–44} (Figure S1H).

The CD-Rhizotron system was then used to analyze the colonization of bacteria along the longitudinal root axis by examining the community structure of discrete root segments. Individual strands of both main and lateral roots were used for subsequent analyses

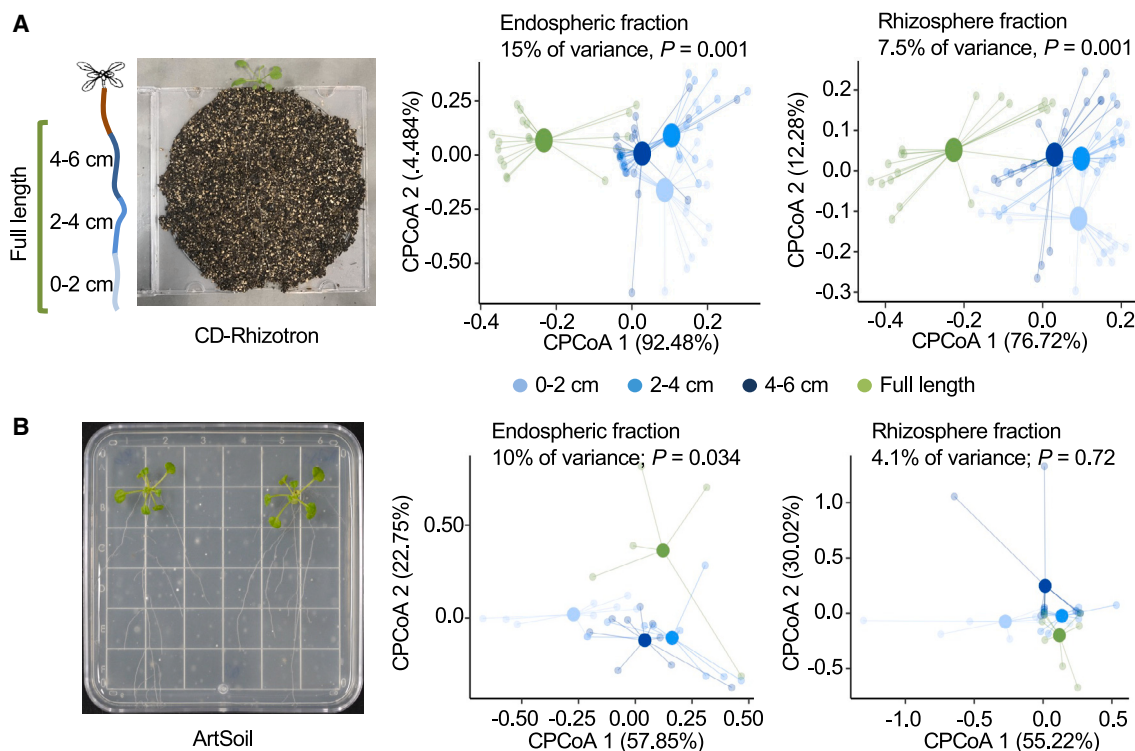


Figure 1. Differential spatial colonization by root microbiota along the longitudinal root axis

(A) Phenotype of wild-type *A. thaliana* Col-0 grown on CD-Rhizotron, with root segments marked. CPCoA of the Bray-Curtis dissimilarities of endospheric ($n = 63$) or rhizosphere samples ($n = 65$), constrained by the distance to the tip from which they were harvested. Different colors represent respective longitudinal segments or whole root samples, with colors of clusters corresponding to the root segments depicted in the plant cartoon. Centroids are indicated for each cluster of root region.

(B) Phenotype of wild-type *A. thaliana* Col-0 grown on ArtSoil. CPCoA of the Bray-Curtis dissimilarities of root endosphere ($n = 39$) or rhizosphere samples ($n = 40$), constrained by the distance to the tip from which they were harvested. Colors of clusters correspond to segments of the root depicted in the plant cartoon. Centroids are indicated for each cluster of root region.

See also Figures S1 and S2.

since the bacterial community profiles of main and lateral roots did not show significant differences (Figure S1I). Roots of 4-week-old plants grown in CD-Rhizotrons were sectioned into 2 cm segments, measuring 0–2, 2–4, and 4–6 cm from the root tip (here on designated as 2, 4, and 6 cm segments, respectively), for bacterial profiling using 16S amplicon sequencing. PCoA of Bray-Curtis dissimilarities constrained by root segment explained 15% of the variation in the endospheric fraction and 7.5% of the variation in the rhizospheric fraction ($p = 0.001$; Figure 1A; Table S1). Thus, we identified a significant separation between samples from the three root segments, indicating dissimilarities between bacterial community structures.

To be able to monitor root growth and simplify root sectioning, an agar-based plant growth system was developed. Typically, plant growth media are supplemented with sucrose or glucose to facilitate seed germination and plant growth. For many plants, including *Arabidopsis*, the sugars are necessary for efficient growth; however, they also impact root physiology and alter microbiota dynamics.^{40,45–47} To enable growth without the unphysiological supplementation with sugars, an ArtSoil system was developed. In this system, plant growth was supported on an agar matrix inoculated with an aqueous soil extract. The phenotype and growth of plants grown on ArtSoil were comparable

to that of plants grown on half-strength Murashige-Skoog ($\frac{1}{2}$ MS-salt) media supplemented with 1% sucrose (Figure S2A).

To determine the adequate amount of soil inoculum for ArtSoil that would recapitulate natural soil bacterial diversity and root colonization, dilution-to-extinction assays were performed by inoculating ArtSoil with 10^{-2} , 10^{-4} , or 10^{-6} dilutions of soil-derived live bacterial suspension (Figure S2B). Rhizobiota analysis using 16S rRNA amplicon sequencing was performed on 3-week-old *A. thaliana* seedlings grown on ArtSoil. ArtSoil made from all three dilutions recapitulated the relative abundance and diversity of the core root microbiome of *A. thaliana* grown on soil,⁴⁴ and the differences in community structures between the three soil dilutions were not significant (Figure S2C). Furthermore, PCoA analysis of Bray-Curtis dissimilarities revealed distinct rhizospheric, endospheric, and bulk agar clusters, similar to that found in roots of soil-grown plants⁴³ (Figure S2D).

To investigate whether ArtSoil could reconstitute the spatial colonization of rhizobiota as found using the CD-Rhizotron system (Figure 1A), dissimilarity matrix ordination analysis was performed on bacterial communities in each segment and for full-length roots. Constrained PCoA of the Bray-Curtis dissimilarities revealed that root segments explained 10% of the variation in the

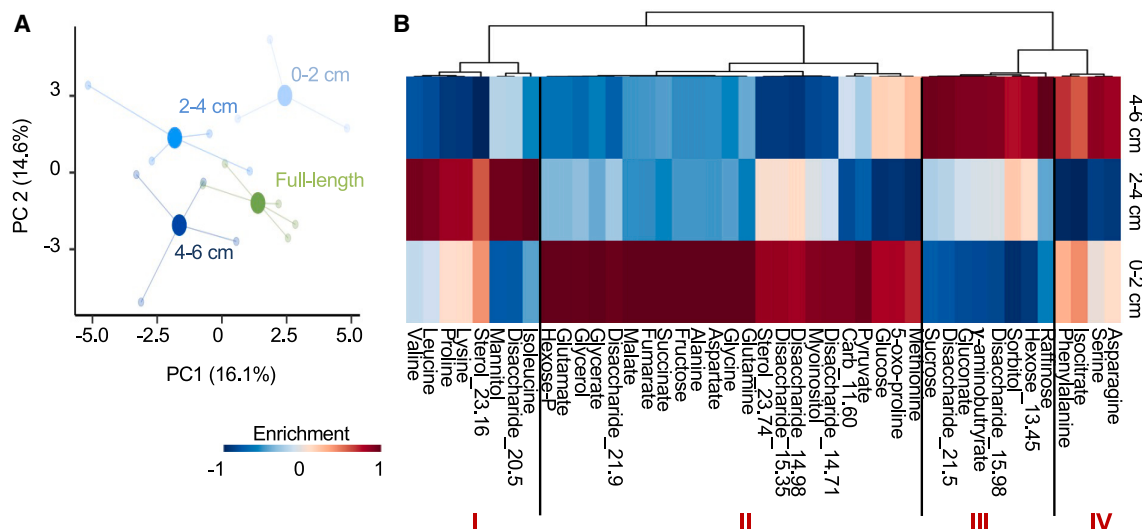


Figure 2. Diversity and region-specificity of metabolites along the root axis

(A) Principal-component analysis (PCA) of metabolites extracted from the full-length root, and segments 0–2, 2–4, and 4–6 cm from the root tip. The colors of clusters correspond to regions of the root depicted in the plant cartoon in Figure 1A. Centroids are indicated for each cluster of root region.

(B) Heatmap depicting the enrichment or depletion of indicated metabolites in respective root segments. Clustering performed based on average linkage Pearson hierarchical clustering of metabolites. Clusters are indicated in red roman numbers. Colors on the scale bar indicate the level of enrichment or depletion of each metabolite across the root segments.

See also Figure S3.

endospheric fraction ($p = 0.034$, Figure 1B; Table S1). Four distinct clusters observed in the endospheric fractions indicated distinct rhizobacteria community structures for each root segment, as observed using the CD-Rhizotron system. However, ArtSoil did not fully reconstitute the spatial colonization pattern of microbiota-derived from the rhizospheric fraction (4.1% of the variation with $p = 0.72$, Figure 1B; Table S1), most likely due to loss of microbiota diversity. The roots of *A. thaliana* grown in gnotobiotic CD-Rhizotron inoculated with a 60-member synthetic microbiota community⁴⁸ (SynCom) exhibited spatial root organization in the endospheric fraction but not the rhizospheric fraction (Figure S2E). Failure to reconstitute spatial rhizospheric colonization from plants grown in ArtSoil and gnotobiotic systems hinted toward a need for high microbiota diversity to establish spatial organization in the “rhizosphere.” Taken together, differential patterning of root-associated microbiota colonization along the longitudinal root axis of *A. thaliana* was identified using two growth systems with natural soil microbiota and a synthetic microbiota community.

Differential enrichment of metabolites along the root longitudinal axis

Since exudation of root metabolites is one of the key processes by which plants interact with soil microbes,²⁰ we hypothesized that spatial differentiation in root colonization could be caused at least in part by differential root metabolism along the root axis. To test this hypothesis, metabolites from full-length roots and segments 2, 4, and 6 cm of seedlings grown on ArtSoil were extracted for untargeted gas chromatography-mass spectrometry analyses. 46 metabolites that had >70% database matches to the National Institute of Standards and Technology (NIST) reference library or a custom in-house library could be identified (Table S4). Metabo-

lites were categorized into four superclasses based on chemical structures in the RefMet reference library.

Principal-component analysis (PCA) of metabolites from the root segments revealed that the 1st and 2nd principal components represented 30.7% of the total variation in the metabolite profiles (Figure 2A). Distinct clusters were observed, with metabolites derived from the same root segment clustering tightly, relative to metabolites derived from other segments. Average linkage hierarchical clustering based on Pearson correlation was performed to visualize the enrichment or depletion of metabolites in each root segment (Figure 2B). The metabolites followed four enrichment patterns: metabolites in cluster II showed a gradient from the 6 cm segment toward the 2 cm segment, while cluster III metabolites showed the reverse pattern. Clusters I and IV did not follow a gradient along the root but rather a segment-specific enrichment, i.e., cluster I metabolites were enriched in the 4 cm segment, while cluster IV metabolites were enriched in segment 6 cm.

Cluster II contained 23 metabolites that were enriched in the root tip (2 cm segment). Of the 23 metabolites, 11 were carbohydrates, 11 were organic acids, and 1 was a sterol lipid. The root tip (2 cm segment) showed the most diverse metabolite pattern, i.e., the highest number of enriched metabolites with even distribution between carbohydrates and organic acids. The 4 cm segment was the least diverse profile with a higher representation of organic acids (cluster I: 7 metabolites, of which 4 were organic acids, 2 carbohydrates, and 1 sterol lipid). The root segment furthest from the tip, i.e., at 6 cm, was enriched for carbohydrates (7 out of 12 metabolites fell into the carbohydrate superclass; clusters III and IV). In sum, metabolite profiling of root segments provided evidence for differentiation in the spatial accumulation of root metabolites, specifically, the presence of

Table 1. SWEETs accumulation along the longitudinal region of roots from *A. thaliana* grown on ½ Murashige-Skoog (½ MS) media supplemented with or without sucrose, and ArtSoil

SWEET	½ MS – sucrose	½ MS + sucrose	ArtSoil
1	regions below 2 cm	regions below 2 cm	regions below 2 cm
2	regions below 0.05 cm and above 2 cm	regions below 0.05 cm and above 2 cm	entire root
3	not tested	not tested	not tested
4	not detected	regions above 2 cm (patchy)	not detected
5	not tested	not tested	not tested
6	not tested	not tested	not tested
7	not detected	not detected	not detected
8	not detected	not detected	not detected
9	not tested	not tested	not tested
10	not tested	not tested	not tested
11	regions below 2 cm	at 2.5–3 cm region	regions below 2 cm
12	regions below 2 cm	regions 2 cm and above	regions 2 cm and above
13	regions below 2.5 cm	regions below 2.5 cm	regions below 2.5 cm
14	not tested	not tested	not tested
15	not tested	not tested	not tested
16	not tested	not tested	not tested
17	entire root	entire root	entire root

metabolite concentration gradients, and segment-specific metabolite enrichment along the longitudinal root axis.

Differential accumulation of SWEET sugar uniporters along the root axis

In vitro studies using bacteria derived from soil and plants, coupled with machine learning, indicated that carbon sources govern community assembly.⁴⁰ Notably, bacterial communities were found to assemble in a similar manner when grown in media with sugar and sugar/organic acid, but more distinct when only organic acids were supplied.⁴⁰ Consistently, a large-scale screening of *A. thaliana* leaf microbiota on 45 carbon sources revealed that sugars are the most commonly used carbon source in the phyllosphere.⁴¹ We therefore hypothesized that interference with sugar sequestration from root cells could provide insight into the mechanism behind spatial colonization. Plants use three main sugar transporter families: SWEETs, STPs (sugar transport proteins), and SUT/SUCs (sucrose transporter/sucrose carriers). SUTs and STPs are H⁺-coupled symporters that take up sucrose or hexose, respectively, from the apoplast into the cytosol, while SWEETs as uniporters enable the release of sugars. The pathway activity scores (PASs) for all sugar-related metabolic pathways in the root were calculated to examine the potential involvement of SWEETs in sugar-related metabolic pathways. Differentiation of sugar metabolism and transport along the root axis was explored by modeling the conversion of sucrose into disaccharides and monosaccharides. The PAS of sugar-related metabolic pathways along the longitudinal axis of *Arabidopsis* roots was computed using publicly available microarray data¹¹ and plant metabolic pathway inventories (AraCyc: <https://plantcyc.org>). The correlation between the transcript level of each SWEET and the activity of each sugar-related metabolic pathway in the root was calculated using Spearman correlation (Figure S3A). Transcript levels of all

SWEETs except SWEET11 were significantly correlated with at least one sugar-related metabolic pathway in the root. Hence, we posited that SWEETs may play a role in root sugar flux. The average RNA levels of each SWEET in each segment of the root indicated that the accumulation of SWEETs in the roots of plants grown on full-strength MS-salt media supplemented with 1% sucrose follows a spatially differentiated pattern (Figure S3B). The mRNA transcripts of SWEET1, 2, 4, 5, 11, and 14 accumulated in the meristematic zone, whereas mRNAs of SWEET3, 8, and 15 accumulated in the elongation zone. mRNA transcripts for most of the SWEETs, i.e., SWEET6, 7, 9, 10, 11, 12, 14, 16, and 17, accumulated in the maturation zone. The *in silico* analysis provided a basis to investigate the roles of SWEET transporters in spatially organized bacteria root colonization.

SWEETs accumulation patterns in roots are impacted by rhizobiota

To evaluate whether the microarray data for SWEETs (Figure S3B) are also reflected in respective protein levels, the accumulation of SWEET transporters was mapped in transgenic plants carrying translational SWEET-uidA reporter gene fusions driven by the native SWEET promoters (*pSWEET:SWEET-GUS*) grown on sterile ½ MS-salt media supplemented with sucrose. Microarray data were comparable to GUS histochemical analysis for SWEET1, 2, 11, 12, 13, and 17-GUS, but not for SWEET4, 7, and 8-GUS (Table 1; Figure S3B). Microarray data indicated accumulation of SWEET4, 7, and 8, mRNA in the meristematic, elongation, and maturation zones, while GUS histochemical analysis showed accumulation of SWEET4-GUS in regions above 2 cm. SWEET7-GUS and SWEET8-GUS proteins were not observed in the root. Notably, however, the microarray data are limited to regions of the root below 0.5 mm. The low correlation between SWEET mRNA and protein levels is consistent

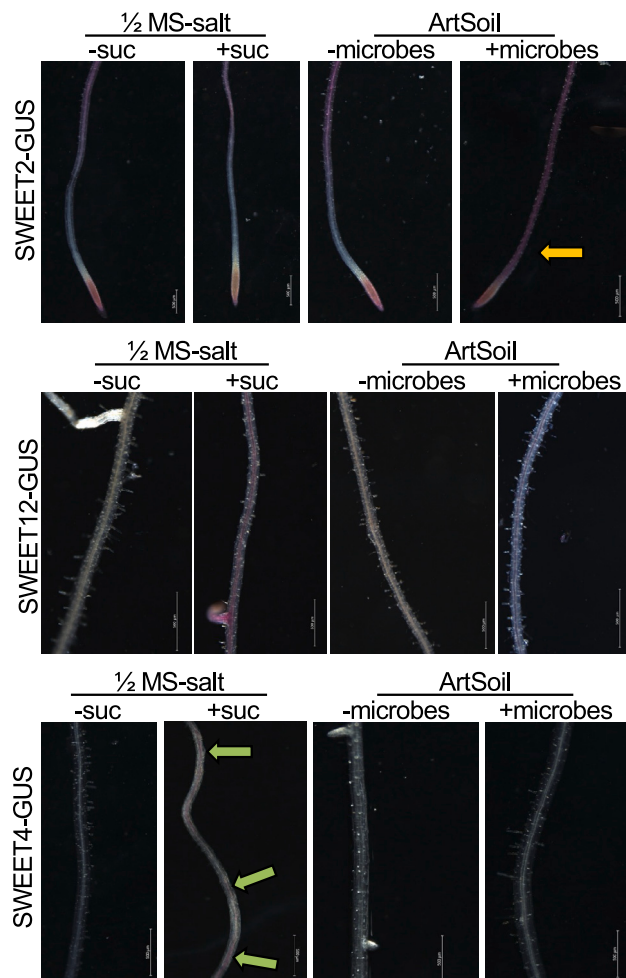


Figure 3. Accumulation of SWEETs along the root in the absence or presence of sugar and soil microbes

Accumulation of respective SWEETs fused with a translational GUS reporter gene in 14-days-old *A. thaliana* seedlings grown on 1/2 MS-salt media supplemented with or without 1% sucrose (1/2 MS-salt –suc: 1/2 MS media without sucrose supplementation, 1/2 MS-salt +suc: 1/2 MS media with sucrose supplementation), on microbiome-inoculated or microbiome-killed ArtSoil (ArtSoil –microbes: ArtSoil inoculated with heat-killed soil microbes, ArtSoil +microbes: ArtSoil inoculated with soil microbes). The root segment depicted for SWEET2-GUS is <0.2 cm, and the root segments depicted for SWEET12-GUS and SWEET4-GUS are >2 cm. Scale bars, 500 μ m. The yellow arrow indicates the accumulation of SWEET2-GUS in the root zone of interest. Green arrows indicate the sporadic accumulation of SWEET4-GUS. Representative image for each genotype from N > 10.

See also Figure S4.

with a generally low correlation between RNA and protein levels for many genes, as, e.g., described in maize.^{49,50}

To evaluate the potential effects of root microbes on SWEET protein levels in the different segments of the root, SWEET-GUS seedlings grown on sterile 1/2 MS-salt media (\pm sucrose) were compared with seedlings grown on ArtSoil (Figures 3 and S4). Histochemical analysis indicated that SWEET2-GUS was comparable all along the root region between 0 and 6 cm in plants grown on ArtSoil. In plants grown on sterile 1/2 MS-salt \pm sucrose and ArtSoil with heat-killed microbes, SWEET2-GUS

accumulated in the root tip (approximately up to 0.05 cm). In the adjacent zone (0.05–0.2 cm), GUS activity was not detectable. SWEET2-GUS was detected upward of this zone (0.2–6 cm). The observed differences in the SWEET2-GUS pattern when comparing ArtSoil and MS media-grown seedlings indicate that microbes exert an effect on SWEET2-GUS in the 0.05–0.2 cm segment. In regions above 2 cm from the root tip, SWEET12-GUS accumulated in the vasculature of plants grown on 1/2 MS-salt with sucrose, but not in roots of plants grown on 1/2 MS-salts without sucrose, nor in ArtSoil with heat-killed microbes. Low levels of SWEET12-GUS were observed in the roots of plants grown on ArtSoil, indicating that both sucrose and microbes lead to elevated SWEET12-GUS levels. Different from SWEET12, SWEET4-GUS accumulated in patches in regions above 2 cm from the root tip in plants grown on 1/2 MS-salts supplemented with sucrose. SWEET4-GUS was neither detected in the absence of sucrose, nor ArtSoil, indicating sugar-dependent accumulation of SWEET4. Taken together, histochemical analyses on SWEET-GUS point to differential effects of sucrose and root microbes on the spatial patterns of SWEET2-GUS, SWEET4-GUS, and SWEET12-GUS.

SWEETs affect spatial colonization of root bacteria

Since the spatial accumulation of SWEET2, SWEET4, and SWEET12 is impacted by microbes (Figure 3; Table 1), metabolite profiles and bacterial colonization of roots of *sweet2*, *sweet4*, and *sweet11;12* mutants were analyzed to investigate the physiological relevance of these SWEET transporters in the spatial patterning of metabolites and rhizobiota. SWEET11 and SWEET12 had previously been reported to serve complementary roles^{51–53}; hence, a *sweet11;12* double knock-out mutant was used for all analyses. Under the conditions used here, *sweet2* and *sweet11;12* mutants grown on ArtSoil did not show growth penalties compared with the wild type (WT) (Figure S5A). PCA on total metabolites from WT and *sweet2*, *sweet4*, and *sweet11;12* roots revealed distinct clusters between WT and *sweet* mutants, but less distinction between the *sweet* mutants (Figure 4A). Despite the tight clustering of metabolite profiles among the three *sweet* mutants, the profiles of individual mutants were distinct (Data S1). Further dissection into metabolites in each segment of the root revealed that only three super-classes, namely organic acids, carbohydrates, and sterol lipids, were significantly altered compared with WT (Figure 4B). A global increase in organic acid levels was observed in all *sweet* mutants.

Pearson average linkage hierarchical clustering revealed five main clusters enriched or depleted depending on the genotype and/or root segment (Figure 4C). Metabolites in clusters I and V exhibited genotype-specific enrichment. Metabolites in cluster V were enriched in WT plants, whereas metabolites in cluster I were enriched in all *sweet* mutants, regardless of the root segment. Clusters II and III showed root segment-specific enrichment across all *sweet* mutants, whereas metabolites in cluster IV were enriched only in the 2 cm segment regardless of plant genotype.

Two-way ANOVA was performed to determine whether the differences in metabolite abundance between WT and *sweet* mutants could be attributed to spatial (2 vs. 4 vs. 6 cm vs. full-length root) or genotypic differences (WT vs. *sweet*). Compared

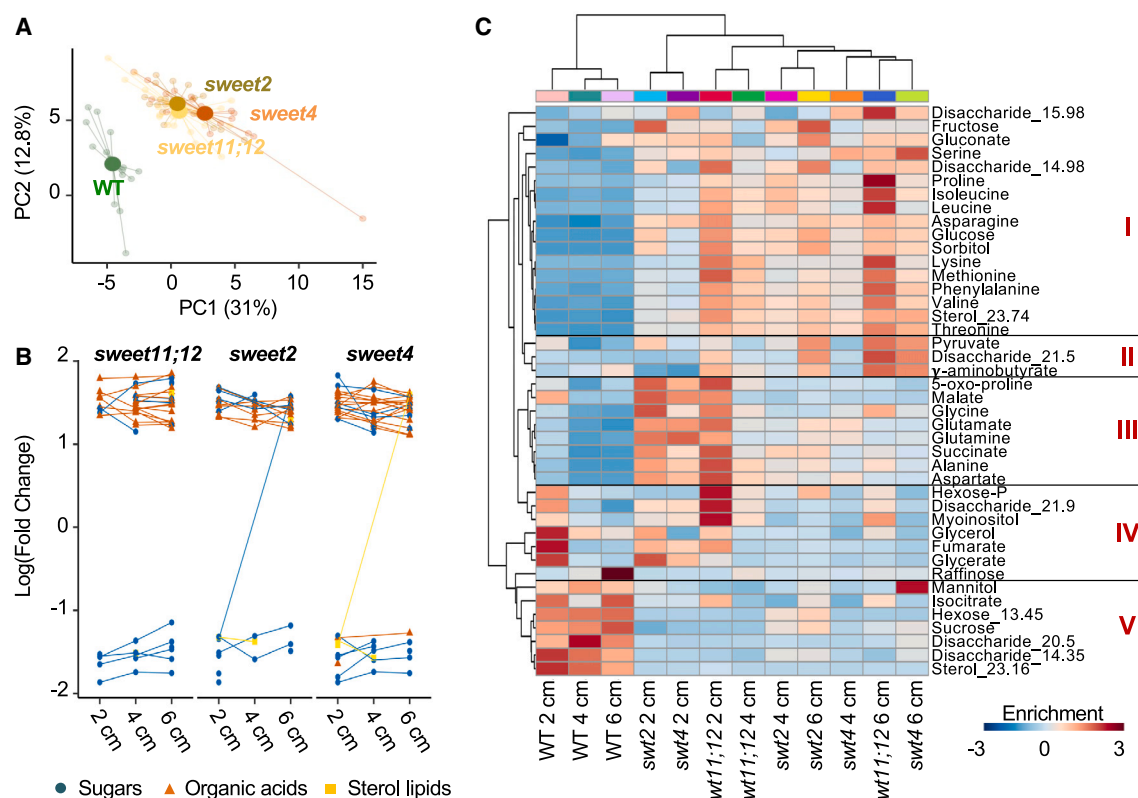


Figure 4. Metabolite profiles of root segments from *sweet2*, *sweet4*, and *sweet11;12* are distinct from WT

(A) Principal-component analysis (PCA) of total metabolites extracted from the whole root and root segments 2, 4, and 6 cm above the root tip of *sweet2*, *sweet4*, *sweet11;12*, and WT plants. WT: N = 16, *sweet2*: N = 19, *sweet4*: N = 20, *sweet11;12*: N = 21.

(B) Relative abundance of metabolite superclasses significantly (p value < 0.05) enriched and depleted in each root segment of *sweet* mutants compared with corresponding segments of WT.

(C) Heatmap depicting the enrichment (or depletion) of indicated metabolites in respective root segments for WT and *sweet* plants (abbreviated as *swt*). Heatmap generated based on average linkage Pearson hierarchical clustering of metabolites and root segments. Clusters are indicated in red roman numbers. Colors indicate the level of enrichment or depletion of each metabolite across the plant genotypes and root segments.

See also Figure S5.

with WT plants, the abundance of disaccharide 14.35 (unidentified) in *sweet2*, mannitol in *sweet4*, and disaccharide 14.35, gluconate, and hexose-P in *sweet11;12* was not caused by spatial or genotype differences (statistically insignificant, $p > 0.05$; Table 2). The abundance of 6–9 carbohydrates (in *sweet2*: 9 metabolites, *sweet4*: 6 metabolites, and *sweet11;12*: 7 metabolites) and 7–8 organic acids (in *sweet2* and *sweet4*: 7 metabolites and *sweet11;12*: 8 metabolites) was caused by spatial differentiation rather than genotypic differences. By comparison, the abundance of 8–14 carbohydrates, 13–14 organic acids, and 1 sterol lipid were attributed to differences in plant genotype. Taken together, the loss of SWEET2, SWEET4, and SWEET11;12 functions led to alterations in the spatial abundance of root metabolites.

Since the ArtSoil system successfully captured endospheric, but not rhizospheric bacterial spatial colonization (Figure 1B), community profiling using 16S amplicon sequencing of *sweet* mutants grown *via* ArtSoil was focused on the endospheric fraction. Community profiling of the root of *sweet2*, *sweet4*, and *sweet11;12* mutants revealed significant differences between *sweet* mutants and WT plants (Kruskal-Wallis, Dunn's test post

hoc, $p = 0.019$; Figure 5A). To determine whether the spatial organization of the endospheric microbiota was retained in the *sweet* mutants, community profiling was performed on segments of root from the mutants. Strikingly, compositional dissimilarities measured using Bray-Curtis distance indicated that bacterial communities from root segments of sweets had lower dissimilarity compared with each other (Figure 5B; Table S1). Bacterial communities from the 2 cm segment of the WT root retained lower (but still distinct, Table S1) Bray-Curtis distance scores compared with 4 and 6 cm segments, indicating differences in the bacterial community between root segments of WT plants. The Bray-Curtis distance scores were higher for root segments of WT compared with corresponding segments in *sweet* mutants (Figures 5B and S5B; Tables S2 and S3), indicating high dissimilarity of bacterial communities between WT and *sweet* mutants. Notably, root segments from *sweet2* and *sweet4* showed insignificant differences in the Bray-Curtis score (Table S1). Spatial organization was retained in *sweet11;12*, but the bacterial communities were different compared with WT plants (Figures S5B; Tables S1–S3). Taken together, the organization of root microbiota along the longitudinal root axis was

Table 2. Contribution of spatial distribution and/or plant genotype to the abundance of root metabolites

Metabolite	Superclass	<i>sweet2</i>	<i>sweet4</i>	<i>sweet11;12</i>
Sterol 23.74	sterol lipid	N/A	N/A	N/A
Sterol 23.16	sterol lipid	genotype	genotype	genotype
Fructose	carbohydrate	genotype	genotype	genotype
Glucose	carbohydrate	genotype	genotype	genotype
Disaccharide 14.98	carbohydrate	genotype	genotype	genotype
Sorbitol	carbohydrate	genotype	genotype	genotype
Sucrose	carbohydrate	genotype	genotype	genotype
Hexose 13.45	carbohydrate	genotype	genotype	genotype
Disaccharide 15.98	carbohydrate	genotype	genotype	genotype
Mannitol	carbohydrate	genotype	N/A	genotype
Disaccharide 14.35	carbohydrate	N/A	genotype	N/A
Gluconate	carbohydrate	genotype, spatial	genotype	N/A
Hexose-P	carbohydrate	spatial	genotype	N/A
Glycerol	carbohydrate	genotype, spatial	genotype	spatial
Carb 11.60	carbohydrate	spatial	spatial	spatial
Disaccharide 21.9	carbohydrate	spatial	genotype	genotype, spatial
Glycerate	carbohydrate	spatial	genotype, spatial	genotype, spatial
5-oxo-Proline	carbohydrate	genotype, spatial	genotype, spatial	genotype, spatial
Disaccharide 21.5	carbohydrate	genotype, spatial	genotype, spatial	genotype, spatial
Raffinose	carbohydrate	genotype, spatial	genotype, spatial	N/A
Disaccharide 14.71	carbohydrate	N/A	N/A	N/A
Disaccharide 20.5	carbohydrate	N/A	N/A	N/A
Myoinositol	carbohydrate	N/A	N/A	N/A
Shikimate	organic oxygen compound	N/A	N/A	N/A
γ -Aminobutyrate	organic acid	N/A	N/A	N/A
Malate	organic acid	spatial	spatial	spatial
Ketoglutarate	organic acid	spatial	spatial	spatial
Fumarate	organic acid	spatial	spatial	spatial
Aspartate	organic acid	genotype, spatial	genotype, spatial	genotype, spatial
Isocitrate	organic acid	genotype, spatial	genotype, spatial	genotype, spatial
Glutamine	organic acid	genotype, spatial	genotype, spatial	genotype, spatial
Alanine	organic acid	genotype	genotype, spatial	genotype, spatial
Glycine	organic acid	genotype, spatial	genotype	genotype
Succinate	organic acid	genotype	genotype	genotype, spatial
Isoleucine	organic acid	genotype	genotype	genotype
Leucine	organic acid	genotype	genotype	genotype
Lysine	organic acid	genotype	genotype	genotype
Asparagine	organic acid	genotype	genotype	genotype
Methionine	organic acid	genotype	genotype	genotype
Phenylalanine	organic acid	genotype	genotype	genotype
Proline	organic acid	genotype	genotype	genotype
Pyruvate	organic acid	genotype	genotype	genotype
Serine	organic acid	genotype	genotype	genotype
Threonine	organic acid	genotype	genotype	genotype
Valine	organic acid	genotype	genotype	genotype
Glutamate	organic acid	genotype	genotype	genotype

N/A: not applicable. The abundance of indicated metabolites is not significantly different from WT plants (two-way ANOVA, $p > 0.05$).

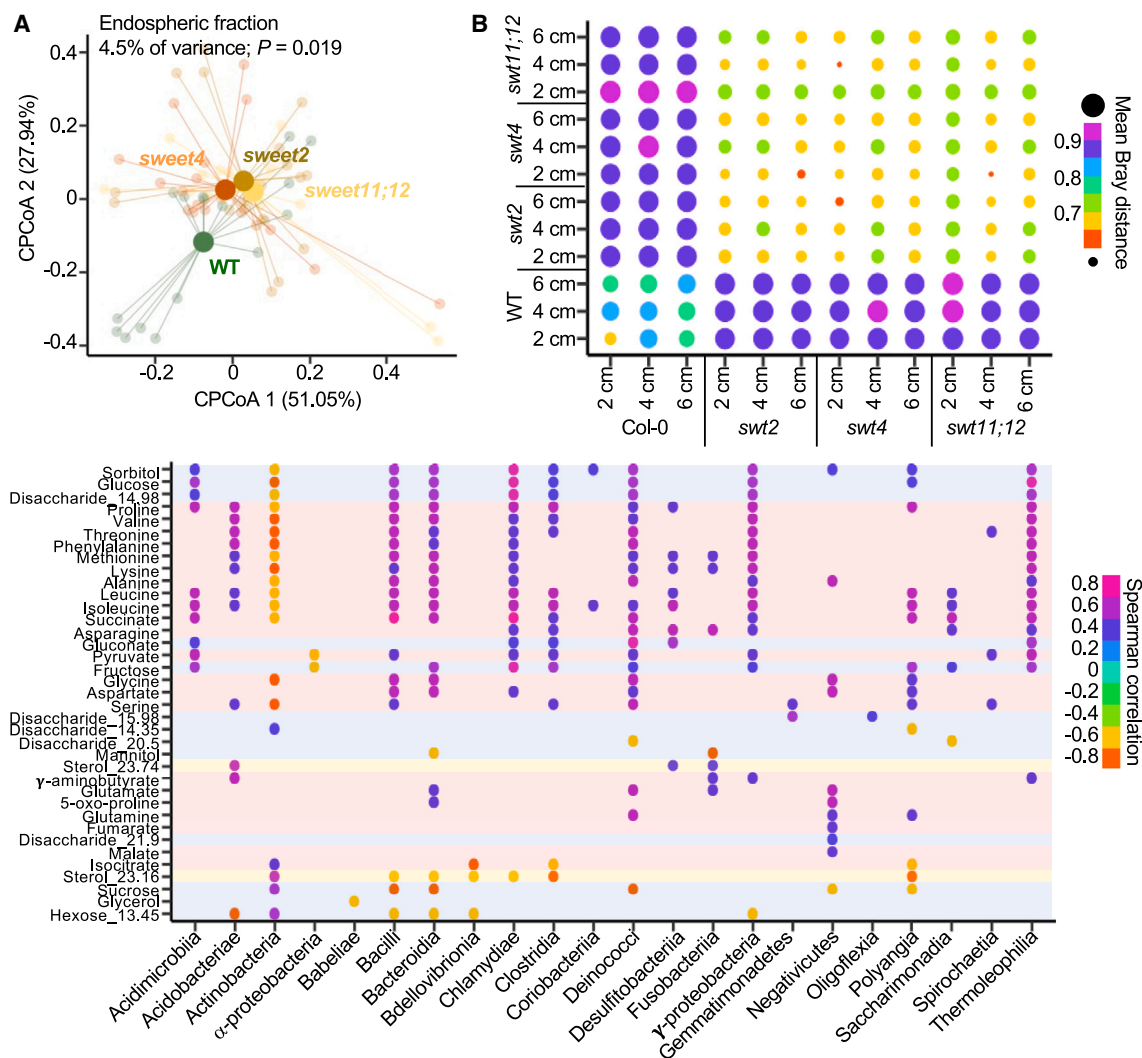


Figure 5. Loss of spatial microbiota colonization in roots of *sweet2*, *sweet4*, and *sweet11;12*

(A) CPCoA of the Bray-Curtis dissimilarities of endospheric bacteria derived from full-length roots of WT, *sweet2*, *sweet4*, and *sweet11;12* plants, constrained by plant genotype. Different colors represent plant genotypes with centroids indicated for each cluster of genotype. WT: N = 60, *sweet2*: N = 40, *sweet4*: N = 41, *sweet11;12*: N = 42.

(B) Bray-Curtis dissimilarities distances of endospheric bacteria derived from the 0–2, 2–4, and 4–6 cm segments from the root tip of WT, *sweet2*, *sweet4*, and *sweet11;12* plants (*sweet* abbreviated as “*swt*”) compared with each other. The colors and sizes of the dots correspond to the mean of the Bray-Curtis distance.

(C) Spearman correlation for metabolite-microbe (class level) pairs. Metabolites ranked based on Spearman average hierarchical clustering. The color of each point indicates the degree of correlation. Highlights indicate the class of metabolite: blue, sugar/carbohydrate; red, organic acid; and yellow, lipid. Spearman correlations significance, $p < 0.05$.

See also Figure S5.

different in *sweet2*, *sweet4*, and *sweet11;12* compared with WT plants. As a control, the root microbiota of *sweet7*, for which SWEET7-GUS accumulation was not detected in the roots, retained its spatial organization along the longitudinal axis of the root (Table 1; Figures S5C and S5D). Collectively, metabolite and microbiota profiling of the *sweet* mutants intimate a role of sugar efflux by SWEET2, 4, and 11;12 along the root as necessary for the spatial organization of root bacteria.

To visualize the relationship between the root microbes and metabolites, correlations between the abundance of microbes and metabolites were computed (Figure 5C). The majority of

the relationships between microbes and metabolites were positive, i.e., an increase in the abundance of metabolite correlated with an increase in the abundance of a specific class of microbes. Most of the metabolites (22 out of 37 metabolites) showed positive and negative relationships with the microbes, 12 metabolites (asparagine, gluconate, aspartate, disaccharide_15.98, sterol_23.74, γ -aminobutyrate, glutamate, 5-oxo-proline, glutamine, fumarate, malate, and disaccharide_21.9) were positively correlated with the microbes only, whereas three metabolites (disaccharide_20.05, glycerol, and mannitol) exclusively had negative relationships with the root microbes. A large

subset of the amino acids had similar relationship patterns with several sugars, i.e., sorbitol, glucose, and disaccharide 14.98, indicating possible interdependence between classes of metabolites (Figures 5C and S5E). Interdependence between sugars and organic acids was also apparent for fructose and pyruvate in which the two metabolites exhibit similar relationship patterns with seven out of nine classes of microbes. In sum, metabolite-microbe correlation analysis unveiled similarities in interaction patterns between metabolite clusters, intimating possible interdependence between metabolites.

DISCUSSION

Here, we developed two plant growth systems that allow tracing of root growth and easy dissection of individual root strands into three longitudinal segments. Bacterial profiling of the three root segments revealed spatial organization (biogeography) of microbiota, i.e., each segment of the root harbors distinct bacterial communities (Figure 1). Metabolite profiling of root segments revealed differential enrichment of metabolites among the three segments (Figure 2). Bioinformatic analysis using publicly available microarray data indicated a high correlation between SWEETs and root sugar metabolic pathways (Figure S3). Accumulation of SWEETs in the root was tested using SWEET-GUS translational fusion plants. SWEET2, SWEET4, and SWEET12 demonstrated spatial differences in the accumulation of proteins in dependence on the presence of soil microbes (Figure 3). Metabolite and microbiota profiling of the roots of *sweet2*, *sweet4*, and *sweet11;12* loss of function mutants showed altered spatial metabolite profiles and disordered spatial bacterial colonization. Collectively, we demonstrated a role for SWEET2, SWEET4, and SWEET11;12 in the overall provision of carbohydrate supply to maintain the spatial organization of root microbiota (Figures 4 and 5).

We surmise that the apparent loss of community structure in the three *sweet* knock-out mutants could be caused by one or several mechanisms: (1) carbon starvation could impact key hub microbes and thus lead to a reduced ability to assemble the three-dimensional biogeography as found in WT roots; (2) the microbes may switch from altruistic community status to egoistic strategies of individuals as described in the “game theory”⁵⁴; or (3) the shift in carbon supply away from carbohydrates to organic and amino acids may affect the overall community assembly. Modeling of resource competition between phyllospheric microbes of *A. thaliana* predicted that competition for sugar between microbes can be alleviated with organic acids supplementation.⁴¹ The roots of *sweet2*, *sweet4*, and *sweet11;12* showed decreased carbohydrate levels concomitant with increased organic acid levels (Figure 4). Alteration in the abundance of organic acids that have been described to play a role in reshaping the root microbiota^{55,56} was observed in the *sweet* mutants. Hence, in *sweet* mutants, organic acids may still support the colonization of root bacteria but result in spatial reorganization. Note however that the communities in the three mutants are not identical, consistent with differences in substrate specificity and expression pattern.

The role of metabolites in shaping community structure

Physiological observations support the function of SWEETs in facilitating sugar influx or efflux in a case-dependent manner.

SWEET12-GUS accumulated in the vasculature in the presence of microbes, indicating phloem unloading to carbon sink caused by bacteria.^{28,57} SWEET2 is a vacuolar transporter, and the GUS histochemistry may indicate a role for sugar sequestration in or transport from the vacuole in the presence of soil microbes.³⁴ The absence of SWEET4-GUS induction in the presence of soil microbes intimates that hexose export into the apoplast is not required in the presence of microbes.⁵⁸ Of note, *sweet4* exhibited a slight growth penalty⁵⁹ (Figure S5A), which could contribute to altered spatial root metabolite and microbiota profiles. In rice and several crop plants, pathogens in the *Xanthomonas* genus inject transcription-activation like (TAL) effectors into host cells to trigger the transcription of SWEETs for SWEET-mediated secretion of sucrose. The secreted sucrose presumably facilitates pathogen feeding and proliferation, leading to disease development.^{28,36,38} Interference with SWEET gene activation confers pathogen resistance.^{37,60–63} In *Arabidopsis*, SWEETs are also involved in various pathogen interactions.^{28,34,58} The spatial distribution of SWEETs along the root could allow plants to control root colonization patterns by nutrient mobilization and/or selective feeding.

The amino acids leucine, arginine, histidine, valine, isoleucine, and tryptophan are required by *Pseudomonas fluorescens* WCS365 for the initial colonization of tomato root tip.⁶⁴ The requirement for multiple amino acids to be present simultaneously (as also seen in Figure 5C) implies a dependency on multiple amino acids to enable successful microbe colonization of the root. Malate, pyroglutamic acid, citric acid, succinate, and fumarate have been shown to be secreted from tomato roots as chemoattractants.⁶⁵ Citric acid, pyruvate, succinate, and fumarate have been implied to play a role in the enrichment of microbes from the *Comamonadaceae* family.⁶⁶ Malate, succinate, and fumarate also serve as energy sources for the establishment of symbiosis.⁶⁷ Metabolite-microbe correlation revealed that pyruvate and fructose exhibit similar relationship patterns, whereas fumarate and malate closely cluster with disaccharide 21.9 (Figures 5C and S5E). The similarity in the relationship patterns among the metabolites hints at the potential role of sugars together with organic acids to affect colonization patterns. Taken together, interdependency exists between sugars and organic acids in shaping the rhizobial colonization patterns. Further inspection into the interdependence among metabolites may provide insights into how metabolite cocktails (e.g., root exudate) shape microbial patterning.

Potential role of immunity-related processes in the host microbiota interaction

The root of *A. thaliana* exhibits spatial differentiation of immune responses. Microbe-associated molecular pattern (MAMP)-trigger immunity (MTI) is confined to the root cap and the transition/elongation zone, whereas immune responses are apparently weaker in differentiated root parts.¹⁶ Screening of 627 *A. thaliana* root commensals from diverse taxonomic origins found diversity in the response to the immunogenic flg22, which elicits antagonistic immune responses.⁶⁸ Flg22 induces enhanced sugar uptake activity from the apoplast via the sugar uniporter STP13.⁶⁹ Microbes also reduce the environmental pH using organic acids to inhibit the flg22-activated immune response.⁷⁰ Taken together, the selective recruitment of microbes along the root could be a strategy to select compatible

bacteria that will co-modulate host susceptibility to pathogens by either eliciting or dampening MTI responses.⁷¹ MTI activation-inactivation buffers the plant immune system against pathogen perturbation and defense-associated growth inhibition, leading to commensal-host homeostasis. Our data indicate that the *sweet* mutants, although with spatial microbiota reorganization, still maintain their overall root microbiota homeostasis, as evident by the absence of growth inhibition compared with WT plants (Figure S5A).

Other host developmental actors

The three root segments selected in this work encompass all stages of root development, i.e., meristematic, elongation, and maturation zones are within 0.05 cm from the root tip.^{72–74} Thus, the differences in metabolite and microbiota profiles among the root segments may not correspond to the developmental stages but possibly to root suberization stages. In the presence of root microbes, full suberization may extend up to 3 cm from the root tip.⁷⁵ The transition from Casparian strip formation to full suberization of the endodermis starts sporadically in a patch-like manner.⁷⁶ Hence, it is plausible that the 2 cm segment represents non-suberized and patchy zones, the 4 cm represents patchy and fully suberized zones, and the 6 cm represents fully suberized root.⁷⁷ The suberization status of the endodermis influences the root colonization of microbes through the secretion of specific root metabolites. In a bidirectional feedback manner, root microbes influence diffusion barrier formation, in turn affecting the balance of mineral nutrients in the plant.⁷⁵

Conclusion and outlook

Similar to animal systems, the microbiota of plant roots are spatially differentiated.⁷⁸ The 2 cm segments used here indicated complex biogeography, however, there is likely a much finer spatial differentiation within these regions, both in the axial and radial axes. This work also highlights the interdependency of host and microbiota regarding metabolic activities. The rhizosphere is defined as the soil typically >2 mm from the root,⁷⁹ whose properties (including microbial activities) are affected by root exudations. Since the rhizosphere of media-grown plants has so far not been determined, we here defined the rhizosphere for plants grown on ArtSoil as the 5 mm region surrounding the root. We show that the endogenous microbes derived from the roots of plants grown on ArtSoil could reconstitute the endogenous microbiota present in soil-grown plants. It will be interesting to also analyze the agar fraction that extends 5 mm from the root surface of plants (the so-called rhizosphere) grown on ArtSoil, and to test whether the communities are affected by root exudation. Three-dimensional (3D)-localization of community members by using fluorescence *in situ* hybridization (FISH) or similar approaches may help to get more detailed information on this zone. At present, microbiota within the segments is treated as a general community; however, in mammalian systems, it has been established that compounds produced by one microbe are used by another, and as a result the existence of complex metabolic pathways across multiple microbiotas. It will be interesting to map out individual interdependencies of microbiota in their respective microdomains in future studies. Further dissection will help to untangle the complex microbiota and advance options to generate functional SynComs. Moreover, the work in-

dicates that we still lack many of the key transporters from the host, such as predicted sugar and organic acid effluxes in the rhizodermis.

STAR★METHODS

Detailed methods are provided in the online version of this paper and include the following:

- **KEY RESOURCES TABLE**
- **RESOURCE AVAILABILITY**
 - Lead contact
 - Materials availability
 - Data and code availability
- **EXPERIMENTAL MODEL**
 - CD-Rhizotron
 - ArtSoil preparation
- **METHOD DETAILS**
 - Construction of translational GUS reporter lines
 - GUS histochemical staining
 - Root metabolite profiling
 - Microbiota profiling
 - DNA extraction and library preparation
- **QUANTIFICATION AND STATISTICAL ANALYSIS**
 - Amplicon sequencing data analysis
 - ANOVA for differential enrichment of metabolites
 - Quantify metabolic activities using PAS
 - Flux balance analysis (FBA) to define pathways
 - Correlation between microbes and metabolites

SUPPLEMENTAL INFORMATION

Supplemental information can be found online at <https://doi.org/10.1016/j.chom.2024.02.014>.

ACKNOWLEDGMENTS

This research has been supported by the Deutsche Forschungsgemeinschaft (DFG, German Research Foundation) under Germany's Excellence Strategy — EXC-2048/1 — project ID 390686111, DFG project ID 391465903/GRK 2466, and the Alexander von Humboldt Professorship to W.B.F. T.Y. Pang was supported by the MODS project funded by the program “Profilbildung 2020” (grant no. PROFILNRW2020-107-A), an initiative of the Ministry of Culture and Science of the State of North Rhine Westphalia. We would like to dedicate this manuscript to Allan C. Spradling, Director emeritus at the Dep. Embryology, Carnegie Institution for Science, whose work on the “Physiological and stem cell compartmentalization within the *Drosophila* midgut” inspired this project.

AUTHOR CONTRIBUTIONS

Conception: E.P.-I.L. and W.B.F. writing: E.P.-I.L. and W.B.F. experiments and data analyses: microbiota: R.G.-O, P.D., C. Durán, and E.P.-I.L.; bioinformatics: T.Y.P., M.L., and E.P.-I.L.; localization: E.P.-I.L. and C. Deng; metabolomics: P.W. and E.P.-I.L.

DECLARATION OF INTERESTS

The authors declare no competing interests.

Received: June 22, 2023
Revised: February 1, 2024
Accepted: February 21, 2024
Published: March 12, 2024

REFERENCES

- Berry, D., Stecher, B., Schintlmeister, A., Reichert, J., Brugiroux, S., Wild, B., Wanek, W., Richter, A., Rauch, I., Decker, T., et al. (2013). Host-compound foraging by intestinal microbiota revealed by single-cell stable isotope probing. *Proc. Natl. Acad. Sci. USA* **110**, 4720–4725.
- O'May, G.A., Reynolds, N., Smith, A.R., Kennedy, A., and Macfarlane, G.T. (2005). Effect of pH and antibiotics on microbial overgrowth in the stomachs and duodena of patients undergoing percutaneous endoscopic gastrostomy feeding. *J. Clin. Microbiol.* **43**, 3059–3065.
- Vaishnav, S., Yamamoto, M., Severson, K.M., Ruhn, K.A., Yu, X., Koren, O., Ley, R., Wakeland, E.K., and Hooper, L.V. (2011). The antibacterial lectin RegIIIγ promotes the spatial segregation of microbiota and host in the intestine. *Science* **334**, 255–258.
- Marianes, A., and Spradling, A.C. (2013). Physiological and stem cell compartmentalization within the *Drosophila* midgut. *eLife* **2**, e00886.
- Bosco-Drayon, V., Poidevin, M., Gomperts Boneca, I., Narbonne-Reveau, K., Julien, R., and Charroux, B. (2012). Peptidoglycan sensing by the receptor PGRP-LE in the *Drosophila* Gut induces immune responses to infectious bacteria and tolerance to microbiota. *Cell Host Microbe* **12**, 153–165.
- Hacquard, S., Garrido-Oter, R., González, A., Spaepen, S., Ackermann, G., Lebeis, S., McHardy, A.C., Dangl, J.L., Knight, R., Ley, R., and Schulze-Lefert, P. (2015). Microbiota and host nutrition across plant and animal kingdoms. *Cell Host Microbe* **17**, 603–616.
- Geldner, N. (2013). The endodermis. *Annu. Rev. Plant Biol.* **64**, 531–558.
- Getzke, F., Hassani, M.A., Crüsemann, M., Malisic, M., Zhang, P., Ishigaki, Y., Böhringer, N., Jiménez Fernández, A., Wang, L., Ordon, J., et al. (2023). Cofunctioning of bacterial exometabolites drives root microbiota establishment. *Proc. Natl. Acad. Sci. USA* **120**, e2221508120.
- Dastogeer, K.M.G., Haque Tumpa, F., Sultana, A., Akter, M.A., and Chakraborty, A. (2020). Plant microbiome—an account of the factors that shape community composition and diversity. *Curr. Plant Biol.* **23**.
- Tropini, C., Earle, K.A., Huang, K.C., and Sonnenburg, J.L. (2017). The gut microbiome: connecting spatial organization to function. *Cell Host Microbe* **21**, 433–442.
- Brady, S.M., Orlando, D.A., Lee, J.-Y., Wang, J.Y., Koch, J., Dinneny, J.R., Mace, D., Ohler, U., and Benfey, P.N. (2007). A high-resolution root spatiotemporal map reveals dominant expression patterns. *Science* **318**, 801–806.
- Chubierre, C., Plancot, B., Driouch, A., Moore, J.P., Bardor, M., Gügi, B., and Vitré, M. (2018). Plant immunity is compartmentalized and specialized in roots. *Front. Plant Sci.* **9**, 1692.
- Denyer, T., Ma, X., Klesen, S., Scacchi, E., Nieselt, K., and Timmermans, M.C.P. (2019). Spatiotemporal developmental trajectories in the Arabidopsis root revealed using high-throughput single-cell RNA sequencing. *Dev. Cell* **48**, 840–852.e5.
- Jean-Baptiste, K., McFaline-Figueroa, J.L., Alexandre, C.M., Dorrity, M.W., Saunders, L., Bubb, K.L., Trapnell, C., Fields, S., Queitsch, C., and Cuperus, J.T. (2019). Dynamics of gene expression in single root cells of *Arabidopsis thaliana*. *Plant Cell* **31**, 993–1011.
- Moussaieff, A., Rogachev, I., Malitsky, S., Toal, T.W., Belcher, H., Yativ, M., Brady, S.M., Benfey, P.N., and Aharoni, A. (2013). High-resolution metabolic mapping of cell types in plant roots. *Proc. Natl. Acad. Sci. USA* **110**, E1232–E1241.
- Zhou, F., Emonet, A., Tendon, V.D., Marhavy, P., Wu, D., Lahaye, T., and Geldner, N. (2020). Co-incidence of damage and microbial patterns controls localized immune responses in roots. *Cell* **180**, 440–453.e18.
- Thiergart, T., Zgadzaj, R., Bozsóki, Z., Garrido-Oter, R., Radutoiu, S., and Schulze-Lefert, P. (2019). *Lotus japonicus* symbiosis genes impact microbial interactions between symbionts and multikingdom commensal communities. *mBio* **10**, e01833-19.
- Yu, P., He, X., Baer, M., Beirinckx, S., Tian, T., Moya, Y.A.T., Zhang, X., Deichmann, M., Frey, F.P., Bresgen, V., et al. (2021). Plant flavones enrich rhizosphere Oxalobacteraceae to improve maize performance under nitrogen deprivation. *Nat. Plants* **7**, 481–499.
- Badri, D.V., Chaparro, J.M., Zhang, R., Shen, Q., and Vivanco, J.M. (2013). Application of natural blends of phytochemicals derived from the root exudates of Arabidopsis to the soil reveal that phenolic-related compounds predominantly modulate the soil microbiome. *J. Biol. Chem.* **288**, 4502–4512.
- Bais, H.P., Weir, T.L., Perry, L.G., Gilroy, S., and Vivanco, J.M. (2006). The role of root exudates in rhizosphere interactions with plants and other organisms. *Annu. Rev. Plant Biol.* **57**, 233–266.
- Badri, D.V., and Vivanco, J.M. (2009). Regulation and function of root exudates. *Plant Cell Environ.* **32**, 666–681.
- Kranawetter, C., Zeng, S., Joshi, T., and Sumner, L.W. (2021). A *Medicago truncatula* metabolite atlas enables the visualization of differential accumulation of metabolites in root tissues. *Metabolites* **11**, 238.
- Hu, L., Robert, C.A.M., Cadot, S., Zhang, X., Ye, M., Li, B., Manzo, D., Chervet, N., Steinger, T., van der Heijden, M.G.A., et al. (2018). Root exudate metabolites drive plant-soil feedbacks on growth and defense by shaping the rhizosphere microbiota. *Nat. Commun.* **9**, 2738.
- Jacoby, R.P., Chen, L., Schwier, M., Koprivova, A., and Koprivova, S. (2020). Recent advances in the role of plant metabolites in shaping the root microbiome. *F1000Res* **9**, 151.
- Schütz, V., Frindte, K., Cui, J., Hacquard, S., Schulze-Lefert, P., Knief, C., Schulz, M., and Dörmann, P. (2021). Differential impact of plant secondary metabolites on the soil microbiota. *Front. Microbiol.* **12**, 666010.
- Jones, D.L., and Murphy, D.V. (2007). Microbial response time to sugar and amino acid additions to soil. *Soil Biol.* **39**, 2178–2182.
- Ortiz-Castro, R., Contreras-Cornejo, H.A., Macías-Rodríguez, L., and López-Bucio, J. (2009). The role of microbial signals in plant growth and development. *Plant Signal. Behav.* **4**, 701–712.
- Chen, L.-Q., Qu, X.-Q., Hou, B.-H., Sosso, D., Osorio, S., Fernie, A.R., and Frommer, W.B. (2012). Sucrose efflux mediated by SWEET proteins as a key step for phloem transport. *Science* **335**, 207–211.
- Feng, L., and Frommer, W.B. (2015). Structure and function of SemiSWEET and SWEET sugar transporters. *Trends Biochem. Sci.* **40**, 480–486.
- An, J., Zeng, T., Ji, C., de Graaf, S., Zheng, Z., Xiao, T.T., Deng, X., Xiao, S., Bisseling, T., Limpens, E., and Pan, Z. (2019). A *Medicago truncatula* SWEET transporter implicated in arbuscule maintenance during arbuscular mycorrhizal symbiosis. *New Phytol.* **224**, 396–408.
- Kim, J.-Y., Loo, E.P.I., Pang, T.Y., Lercher, M., Frommer, W.B., and Wudick, M.M. (2021). Cellular export of sugars and amino acids: role in feeding other cells and organisms. *Plant Physiol.* **187**, 1893–1914.
- Manck-Götzenberger, J., and Requena, N. (2016). Arbuscular mycorrhiza symbiosis induces a major transcriptional reprogramming of the potato SWEET sugar transporter family. *Front. Plant Sci.* **7**, 487.
- Sugiyama, A., Saida, Y., Yoshimizu, M., Takanashi, K., Sosso, D., Frommer, W.B., and Yazaki, K. (2017). Molecular characterization of LjSWEET3, a sugar transporter in nodules of *Lotus japonicus*. *Plant Cell Physiol.* **58**, 298–306.
- Chen, H.-Y., Huh, J.-H., Yu, Y.-C., Ho, L.-H., Chen, L.-Q., Tholl, D., Frommer, W.B., and Guo, W.-J. (2015). The Arabidopsis vacuolar sugar transporter SWEET2 limits carbon sequestration from roots and restricts *Pythium* infection. *Plant J.* **83**, 1046–1058.
- Breia, R., Conde, A., Badim, H., Fortes, A.M., Gerós, H., and Granell, A. (2021). Plant SWEETs: from sugar transport to plant-pathogen interaction and more unexpected physiological roles. *Plant Physiol.* **186**, 836–852.
- Cox, K.L., Meng, F., Wilkins, K.E., Li, F., Wang, P., Booher, N.J., Carpenter, S.C.D., Chen, L.-Q., Zheng, H., Gao, X., et al. (2017). TAL effector driven induction of a SWEET gene confers susceptibility to bacterial blight of cotton. *Nat. Commun.* **8**, 15588.
- Oliva, R., Ji, C., Atienza-Grande, G., Huguet-Tapia, J.C., Perez-Quintero, A., Li, T., Eom, J.-S., Li, C., Nguyen, H., Liu, B., et al. (2019).

Broad-spectrum resistance to bacterial blight in rice using genome editing. *Nat. Biotechnol.* 37, 1344–1350.

38. Cohn, M., Bart, R.S., Shybut, M., Dahlbeck, D., Gomez, M., Morbitzer, R., Hou, B.-H., Frommer, W.B., Lahaye, T., and Staskawicz, B.J. (2014). *Xanthomonas axonopodis* virulence is promoted by a Transcription Activator-Like Effector-mediated induction of a SWEET sugar transporter in cassava. *Mol. Plant Microbe Interact.* 27, 1186–1198.
39. Tian, T., Sun, B., Shi, H., Gao, T., He, Y., Li, Y., Liu, Y., Li, X., Zhang, L., Li, S., et al. (2021). Sucrose triggers a novel signaling cascade promoting *Bacillus subtilis* rhizosphere colonization. *ISME J.* 15, 2723–2737.
40. Estrela, S., Sanchez-Gorostiaga, A., Vila, J.C., and Sanchez, A. (2021). Nutrient dominance governs the assembly of microbial communities in mixed nutrient environments. *eLife* 10, e65948.
41. Schäfer, M., Pacheco, A.R., Künzler, R., Bortfeld-Miller, M., Field, C.M., Vayena, E., Hatzimanikatis, V., and Vorholt, J.A. (2023). Metabolic interaction models recapitulate leaf microbiota ecology. *Science* 381, eadf5121.
42. Bulgarelli, D., Rott, M., Schlaeppi, K., Ver Loren van Themaat, E., Ahmadinejad, N., Assenza, F., Rauf, P., Huettel, B., Reinhardt, R., Schmelzer, E., et al. (2012). Revealing structure and assembly cues for *Arabidopsis* root-inhabiting bacterial microbiota. *Nature* 488, 91–95.
43. Lundberg, D.S., Lebeis, S.L., Paredes, S.H., Yourstone, S., Gehring, J., Malfatti, S., Tremblay, J., Engelbrektson, A., Kunin, V., del Rio, T.G., et al. (2012). Defining the core *Arabidopsis thaliana* root microbiome. *Nature* 488, 86–90.
44. Trivedi, P., Leach, J.E., Tringe, S.G., Sa, T., and Singh, B.K. (2020). Plant-microbiome interactions: from community assembly to plant health. *Nat. Rev. Microbiol.* 18, 607–621.
45. Cabrera, J., Conesa, C.M., and Pozo, J.C. (2022). May the dark be with roots: a perspective on how root illumination may bias *in vitro* research on plant–environment interactions. *New Phytol.* 233, 1988–1997.
46. Estrela, S., Vila, J.C.C., Lu, N., Bajić, D., Rebolledo-Gómez, M., Chang, C.-Y., Goldford, J.E., Sanchez-Gorostiaga, A., and Sánchez, Á. (2022). Functional attractors in microbial community assembly. *Cell Syst.* 13, 29–42.e7.
47. Shulze, C.N., Cole, B.J., Ciobanu, D., Lin, J., Yoshinaga, Y., Gouran, M., Turco, G.M., Zhu, Y., O'Malley, R.C., and Brady, S.M. (2019). High-throughput single-cell transcriptome profiling of plant cell types. *Cell Rep.* 27, 2241–2247.e4.
48. Bai, Y., Müller, D.B., Srinivas, G., Garrido-Oter, R., Potthoff, E., Rott, M., Dombrowski, N., Münch, P.C., Spaepen, S., Remus-Emsermann, M., et al. (2015). Functional overlap of the *Arabidopsis* leaf and root microbiota. *Nature* 528, 364–369.
49. Walley, J.W., Shen, Z., Sartor, R., Wu, K.J., Osborn, J., Smith, L.G., and Briggs, S.P. (2013). Reconstruction of protein networks from an atlas of maize seed proteotypes. *Proc. Natl. Acad. Sci. USA* 110, E4808–E4817.
50. Walley, J.W., Sartor, R.C., Shen, Z., Schmitz, R.J., Wu, K.J., Urich, M.A., Nery, J.R., Smith, L.G., Schnable, J.C., and Ecker, Joseph.R. (2016). Integration of omic networks in a developmental atlas of maize. *Science* 353, 814–818.
51. Walerowski, P., Gündel, A., Yahaya, N., Truman, W., Sobczak, M., Olszak, M., Rolfe, S., Borisjuk, L., and Malinowski, R. (2018). Clubroot disease stimulates early steps of phloem differentiation and recruits SWEET sucrose transporters within developing galls. *Plant Cell* 30, 3058–3073.
52. Gebauer, P., Korn, M., Engelsdorf, T., Sonnewald, U., Koch, C., and Voll, L.M. (2017). Sugar accumulation in leaves of *Arabidopsis sweet11/sweet12* double mutants enhances priming of the salicylic acid-mediated defense response. *Front. Plant Sci.* 8, 1378.
53. Desrut, A., Moumen, B., Thibault, F., Le Hir, R., Coutos-Thévenot, P., and Vriet, C. (2020). Beneficial rhizobacteria *Pseudomonas simiae* WCS417 induce major transcriptional changes in plant sugar transport. *J. Exp. Bot.* 71, 7301–7315.
54. Zomorodi, A.R., and Segrè, D. (2017). Genome-driven evolutionary game theory helps understand the rise of metabolic interdependencies in microbial communities. *Nat. Commun.* 8, 1563.
55. Badri, D.V., Quintana, N., El Kassis, E.G., Kim, H.K., Choi, Y.H., Sugiyama, A., Verpoorte, R., Martinoia, E., Manter, D.K., and Vivanco, J.M. (2009). An ABC transporter mutation alters root exudation of phytochemicals that provoke an overhaul of natural soil microbiota. *Plant Physiol.* 151, 2006–2017.
56. Kawasaki, A., Dennis, P.G., Forstner, C., Raghavendra, A.K.H., Mathesius, U., Richardson, A.E., Delhaize, E., Gilliam, M., Watt, M., and Ryan, P.R. (2021). Manipulating exudate composition from root apices shapes the microbiome throughout the root system. *Plant Physiol.* 187, 2279–2295.
57. Kuzakov, Y., and Jones, D. (2006). Glucose uptake by maize roots and its transformation in the rhizosphere. *Soil Biol. Biochem.* 38, 851–860.
58. Chong, J., Piron, M.-C., Meyer, S., Merdinoglu, D., Bertsch, C., and Mestre, P. (2014). The SWEET family of sugar transporters in grapevine: VvSWEET4 is involved in the interaction with *Botrytis cinerea*. *J. Exp. Bot.* 65, 6589–6601.
59. Liu, X., Zhang, Y., Yang, C., Tian, Z., and Li, J. (2016). AtSWEET4, a hexose facilitator, mediates sugar transport to axial sinks and affects plant development. *Sci. Rep.* 6, 24563.
60. Xu, Z., Xu, X., Gong, Q., Li, Z., Li, Y., Wang, S., Yang, Y., Ma, W., Liu, L., Zhu, B., et al. (2019). Engineering broad-spectrum bacterial blight resistance by simultaneously disrupting variable TALE-binding elements of multiple susceptibility genes in rice. *Mol. Plant* 12, 1434–1446.
61. Li, T., Liu, B., Spalding, M.H., Weeks, D.P., and Yang, B. (2012). High-efficiency TALEN-based gene editing produces disease-resistant rice. *Nat. Biotechnol.* 30, 390–392.
62. Blanvillain-Baufumé, S., Reschke, M., Solé, M., Auguy, F., Doucoure, H., Szurek, B., Meynard, D., Portefaix, M., Cunnac, S., Guiderdoni, E., et al. (2017). Targeted promoter editing for rice resistance to *Xanthomonas oryzae* pv. *oryzae* reveals differential activities for SWEET14-inducing TAL effectors. *Plant Biotechnol. J.* 15, 306–317.
63. Liu, Q., Yuan, M., Zhou, Y., Li, X., Xiao, J., and Wang, S. (2011). A paralog of the MtN3/saliva family recessively confers race-specific resistance to *Xanthomonas oryzae* in rice: MtN3/saliva-type gene in rice disease resistance. *Plant Cell Environ.* 34, 1958–1969.
64. Simons, M., Permentier, H.P., De Weger, L.A., Wijffelman, C.A., and Lugtenberg, B.J.J. (1997). Amino acid synthesis is necessary for tomato root colonization by *Pseudomonas fluorescens* strain WCS365. *MPMI* 10, 102–106.
65. De Weert, S., Vermeiren, H., Mulders, I.H.M., Kuiper, I., Hendrickx, N., Bloemberg, G.V., Vanderleyden, J., De Mot, R., and Lugtenberg, B.J.J. (2002). Flagella-driven chemotaxis towards exudate components is an important trait for tomato root colonization by *Pseudomonas fluorescens*. *Mol. Plant. Microbe Interact.* 15, 1173–1180.
66. Wen, T., Yuan, J., He, X., Lin, Y., Huang, Q., and Shen, Q. (2020). Enrichment of beneficial cucumber rhizosphere microbes mediated by organic acid secretion. *Hortic. Res.* 7, 154.
67. Udvardi, M.K., and Day, D.A. (1997). Metabolite transport across symbiotic membranes of legume nodules. *Annu. Rev. Plant Physiol. Plant Mol. Biol.* 48, 493–523.
68. Colaïanni, N.R., Parys, K., Lee, H.-S., Conway, J.M., Kim, N.H., Edelbacher, N., Mucyn, T.S., Madalinski, M., Law, T.F., Jones, C.D., et al. (2021). A complex immune response to flagellin epitope variation in commensal communities. *Cell Host Microbe* 29, 635–649.e9.
69. Yamada, K., Saijo, Y., Nakagami, H., and Takano, Y. (2016). Regulation of sugar transporter activity for antibacterial defense in *Arabidopsis*. *Science* 354, 1427–1430.
70. Yu, K., Liu, Y., Tichelaar, R., Savant, N., Lagendijk, E., van Kuijk, S.J.L., Stringlis, I.A., van Dijken, A.J.H., Pieterse, C.M.J., Bakker, P.A.H.M., et al. (2019). Rhizosphere-associated *Pseudomonas* suppress local

root immune responses by gluconic acid-mediated lowering of environmental pH. *Curr. Biol.* 29, 3913–3920.e4.

71. Ma, K.-W., Niu, Y., Jia, Y., Ordon, J., Copeland, C., Emonet, A., Geldner, N., Guan, R., Stolze, S.C., Nakagami, H., et al. (2021). Coordination of microbe–host homeostasis by crosstalk with plant innate immunity. *Nat. Plants* 7, 814–825.
72. Shahan, R., Hsu, C.-W., Nolan, T.M., Cole, B.J., Taylor, I.W., Greenstreet, L., Zhang, S., Afanassiev, A., Vlot, A.H.C., Schiebinger, G., et al. (2022). A single-cell *Arabidopsis* root atlas reveals developmental trajectories in wild-type and cell identity mutants. *Dev. Cell* 57, 543–560.e9.
73. Dolan, L., Janmaat, K., Willemsen, V., Linstead, P., Poethig, S., Roberts, K., and Scheres, B. (1993). Cellular organisation of the *Arabidopsis thaliana* root. *Development* 119, 71–84.
74. Birnbaum, K., Shasha, D.E., Wang, J.Y., Jung, J.W., Lambert, G.M., Galbraith, D.W., and Benfey, P.N. (2003). A gene expression map of the *Arabidopsis* root. *Science* 302, 1956–1960.
75. Salas-González, I., Rey, G., Flis, P., Custódio, V., Gopalchan, D., Bakhoum, N., Dew, T.P., Suresh, K., Franke, R.B., Dangl, J.L., et al. (2021). Coordination between microbiota and root endodermis supports plant mineral nutrient homeostasis. *Science* 371, eabd0695.
76. Haas, D.L., and Carothers, Z.B. (1975). Some ultrastructural observations on endodermal cell development in *Zea mays* roots. *Am. J. Bot.* 62, 336–348.
77. Durr, J., Rey, G., Spaepen, S., Hilton, S., Meehan, C., Qi, W., Kamiya, T., Flis, P., Dickinson, H.G., Feher, A., et al. (2021). A novel signaling pathway required for *Arabidopsis* endodermal root organization shapes the rhizosphere microbiome. *Plant Cell Physiol.* 62, 248–261.
78. Mondragón-Palomino, O., Pocevičiute, R., Lignell, A., Griffiths, J.A., Takko, H., and Ismagilov, R.F. (2022). Three-dimensional imaging for the quantification of spatial patterns in microbiota of the intestinal mucosa. *Proc. Natl. Acad. Sci. USA* 119, e2118483119.
79. York, L.M., Carminati, A., Mooney, S.J., Ritz, K., and Bennett, M.J. (2016). The holistic rhizosphere: integrating zones, processes, and semantics in the soil influenced by roots. *J. Exp. Bot.* 67, 3629–3643.
80. Guo, W.-J., Nagy, R., Chen, H.-Y., Pfrunder, S., Yu, Y.-C., Santelia, D., Frommer, W.B., and Martinoia, E. (2014). SWEET17, a facilitative transporter, mediates fructose transport across the tonoplast of *Arabidopsis* roots and leaves. *Plant Physiol.* 164, 777–789.
81. Yang, J., Luo, D., Yang, B., Frommer, W.B., and Eom, J. (2018). SWEET11 and 15 as key players in seed filling in rice. *New Phytol.* 218, 604–615.
82. Durán, P., Thiergart, T., Garrido-Oter, R., Agler, M., Kemen, E., Schulze-Lefert, P., and Hacquard, S. (2018). Microbial interkingdom interactions in roots promote *Arabidopsis* survival. *Cell* 175, 973–983.e14.
83. Korenblum, E., Dong, Y., Szymanski, J., Panda, S., Jozwiak, A., Massalha, H., Meir, S., Rogachev, I., and Aharoni, A. (2020). Rhizosphere microbiome mediates systemic root metabolite exudation by root-to-root signaling. *Proc. Natl. Acad. Sci. USA* 117, 3874–3883.
84. Gu, Y. (2012). Multicomponent reactions in unconventional solvents: state of the art. *Green Chem.* 14, 2091.
85. Shim, S.-H., Lee, S.-K., Lee, D.-W., Brilhaus, D., Wu, G., Ko, S., Lee, C.-H., Weber, A.P.M., and Jeon, J.-S. (2019). Loss of function of rice plastidic glycolate/glycerate translocator 1 impairs photorespiration and plant growth. *Front. Plant Sci.* 10, 1726.
86. Chambers, M.C., Maclean, B., Burke, R., Amodei, D., Ruderman, D.L., Neumann, S., Gatto, L., Fischer, B., Pratt, B., Egerton, J., et al. (2012). A cross-platform toolkit for mass spectrometry and proteomics. *Nat. Biotechnol.* 30, 918–920.
87. Lommen, A., and Kools, H.J. (2012). MetAlign 3.0: performance enhancement by efficient use of advances in computer hardware. *Metabolomics* 8, 719–726.
88. Thiergart, T., Durán, P., Ellis, T., Vannier, N., Garrido-Oter, R., Kemen, E., Roux, F., Alonso-Blanco, C., Ågren, J., Schulze-Lefert, P., and Hacquard, S. (2020). Root microbiota assembly and adaptive differentiation among European *Arabidopsis* populations. *Nat. Ecol. Evol.* 4, 122–131.
89. Bolyen, E., Rideout, J.R., Dillon, M.R., Bokulich, N.A., Abnet, C.C., Al-Ghalith, G.A., Alexander, H., Alm, E.J., Arumugam, M., Asnicar, F., et al. (2019). Reproducible, interactive, scalable and extensible microbiome data science using QIIME 2. *Nat. Biotechnol.* 37, 852–857.
90. Magoč, T., and Salzberg, S.L. (2011). FLASH: fast length adjustment of short reads to improve genome assemblies. *Bioinformatics* 27, 2957–2963.
91. Callahan, B.J., McMurdie, P.J., Rosen, M.J., Han, A.W., Johnson, A.J.A., and Holmes, S.P. (2016). DADA2: High-resolution sample inference from Illumina amplicon data. *Nat. Methods* 13, 581–583.
92. Seabold, S., and Perktold, J. (2010). Statsmodels: Econometric and statistical modeling with Python. In *Proceedings of the Python in Science Conference*, pp. 92–96.
93. Girden, E. (1992). ANOVA (SAGE Publications, Inc.).
94. Xiao, Z., Dai, Z., and Locasale, J.W. (2019). Metabolic landscape of the tumor microenvironment at single cell resolution. *Nat. Commun.* 10, 3763.
95. Kim, J.-Y., Symeonidi, E., Pang, T.Y., Denyer, T., Weidauer, D., Bezruczyk, M., Miras, M., Zöllner, N., Hartwig, T., Wudick, M.M., et al. (2021). Distinct identities of leaf phloem cells revealed by single cell transcriptomics. *Plant Cell* 33, 511–530.
96. Hawkins, C., Ginzburg, D., Zhao, K., Dwyer, W., Xue, B., Xu, A., Rice, S., Cole, B., Paley, S., Karp, P., and Rhee, S.Y. (2021). Plant Metabolic Network 15: A resource of genome-wide metabolism databases for 126 plants and algae. *J. Integr. Plant Biol.* 63, 1888–1905.
97. Robinson, M.D., and Oshlack, A. (2010). A scaling normalization method for differential expression analysis of RNA-seq data. *Genome Biol.* 11, R25.
98. Robinson, M.D., McCarthy, D.J., and Smyth, G.K. (2010). edgeR: a Bioconductor package for differential expression analysis of digital gene expression data. *Bioinformatics* 26, 139–140.
99. Orth, J.D., Thiele, I., and Palsson, B.Ø. (2010). What is flux balance analysis? *Nat. Biotechnol.* 28, 245–248.
100. de Oliveira Dal'Molin, C.G., Quek, L.-E., Palfreyman, R.W., Brumby, S.M., and Nielsen, L.K. (2009). AraGEM, a genome-scale reconstruction of the primary metabolic network in *Arabidopsis*. *Plant Physiol.* 152, 579–589.
101. Ebrahim, A., Lerman, J.A., Palsson, B.O., and Hyduke, D.R. (2013). COBRApy: COstraints-Based Reconstruction and Analysis for Python. *BMC Syst. Biol.* 7, 74.
102. Holzhütter, H.-G. (2004). The principle of flux minimization and its application to estimate stationary fluxes in metabolic networks: Flux minimization. *Eur. J. Biochem.* 271, 2905–2922.
103. Reznik, E., Mehta, P., and Segrè, D. (2013). Flux imbalance analysis and the sensitivity of cellular growth to changes in metabolite pools. *PLOS Comput. Biol.* 9, e1003195.
104. Csárdi, G., Nepusz, T., Müller, K., Horvát, S., Traag, V., Zanini, F., and Noom, D. (2023). igraph for R: R interface of the igraph library for graph theory and network analysis, Version v1.5.0 (Zenodo). <https://doi.org/10.5281/ZENODO.7682609>.
105. Raghavan, U.N., Albert, R., and Kumara, S. (2007). Near linear time algorithm to detect community structures in large-scale networks. *Phys. Rev. E Stat. Nonlin. Soft Matter Phys.* 76, 36106.

STAR★METHODS

KEY RESOURCES TABLE

REAGENT or RESOURCE	SOURCE	IDENTIFIER
Biological Samples		
<i>Arabidopsis thaliana</i> Col-0 P _{SWEET17} :SWEET17-GUS	Guo et al. ⁸⁰	N/A
<i>Arabidopsis thaliana</i> Col-0 P _{SWEET2} :SWEET2-GUS	Chen et al. ³⁴	N/A
<i>Arabidopsis thaliana</i> Col-0 P _{SWEET12} :SWEET12-GUS	Chen et al. ²⁸	N/A
<i>Arabidopsis thaliana</i> Col-0 P _{SWEET11} :SWEET11-GUS	Chen et al. ²⁸	N/A
<i>Arabidopsis thaliana</i> Col-0 sweet2c	SIGnAL http://signal.salk.edu/	SALK_048430.36.85.x
<i>Arabidopsis thaliana</i> Col-0 sweet11;12	Arabidopsis Biological Resource Center https://abrc.osu.edu	TAIR Germplasm: CS68845
<i>Arabidopsis thaliana</i> Col-0 sweet4a	SIGnAL http://signal.salk.edu/	SALK_072225.23.65.x
Chemicals, Peptides, and Recombinant Proteins		
DFS-Taq DNA polymerase	Bioron	Cat # 101005
Antarctic phosphatase	New England BioLabs	Cat # M0289
Exonuclease I	New England BioLabs	Cat # M0293
Ribitol	Sigma-Aldrich	Cat # PHR3526
Murashige&Skoog media including MES buffer	Duchefa Biochemie	Cat # M0254
Triton™ X-100, for molecular biology	Sigma-Aldrich	Cat # T8787
Agar	Sigma-Aldrich	Cat # 05040
Hygromycin B	Carl Roth	Cat # CP12.2
Thermo Scientific X Gluc	Thermo Fisher Scientific	Cat # R0851
Critical Commercial Assays		
FastDNA™ SPIN Kit for Soil	MP Biomedicals	Cat # SKU116560200-CF
NuceloSpin Soil Mini kit for DNA from soil	Macherey-Nagel	Cat # 740780
QIAquick gel extraction kit	Qiagen	Cat # 28706X4
Quant-iT™ PicoGreen™	Invitrogen	Cat # P7581
Gateway™ LR Clonase™ Enzyme mix	Invitrogen	Cat # 11791019
Deposited Data		
16S sequencing data	This paper	https://www.ebi.ac.uk/ena/browser/home (Accession number: PRJEB63568)
Metabolomics data	This paper	https://www.metabolomicsworkbench.org/ (Study ID: ST002779)
<i>Arabidopsis</i> root spatial microarray	[https://doi.org/10.1126/science.1146265]	GEO dataset: GSE8934 ID: 200008934
NIST14 Mass Spectral Library	https://www.nist.gov/srd/nist-standard-reference-database-1a-v14	N/A
<i>Arabidopsis thaliana</i> Col-0 metabolic pathways	https://pmn.plantcyc.org/organism-summary?object=ARA	N/A
Experimental Models: Organisms/Strains		
<i>Arabidopsis thaliana</i> Col-0	TAIR	TAIR accession Germplasm:1008804532

(Continued on next page)

Continued

REAGENT or RESOURCE	SOURCE	IDENTIFIER
Oligonucleotides		
AtSWEET4-Xbal-F	IDT	GCAGGTCGACTCTAGAAGTGGTTCCACG GAGATGACG
AtSWEET4-BamHI-R	IDT	CGGTACCCGGGGATCCAGCTGAAACTCG TTTAGCTTGTCC
AtSWEET5-Xbal-F	IDT	GCAGGTCGACTCTAGATTAGGACTGACAC CAGCGATGC
AtSWEET5-BamHI-R	IDT	CGGTACCCGGGGATCCAGCCTGGCCAAG TTCGATTC
AtSWEET7-Xbal-F	IDT	GCAGGTCGACTCTAGAATTGAGGCTTGGC GTAACCTTG
AtSWEET7-BamHI-R	IDT	CGGTACCCGGGGATCCAACATTGTTAGGT TCTTGTTGG
AtSWEET8-Xbal-F	IDT	GCAGGTCGACTCTAGAACCATGACAATTT GGCTCCGAG
AtSWEET8-BamHI-R	IDT	CGGTACCCGGGGATCCAACCCTCTCCGT AGCAGAAATC
Recombinant DNA		
pMDC163 vector	<i>Arabidopsis</i> Biological Resource Center https://abrc.osu.edu	TAIR accession Vector:1009003758
promoterless GUSplus vector	Yang et al. ⁸¹	N/A
Software and Algorithms		
iGraph	https://CRAN.R-project.org/package=igraph	RRID:SCR_019225
COBRAPy	http://opencobra.sourceforge.net	RRID:SCR_012096
GUROBI	https://www.gurobi.com/	N/A
statsmodels	https://www.statsmodels.org/stable/index.html	RRID:SCR_016074
Vegan	https://cran.r-project.org/web/packages/vegan/index.html	RRID:SCR_011950
Qiime2	https://qiime2.org/	RRID:SCR_008249
Flash2	https://github.com/dstreett/FLASH2	RRID:SCR_005531
Dada2	https://benjineb.github.io/dada2	RRID:SCR_008205
Others		
16S data analyses	This work	GitHub https://github.com/duranpa/sweet_collaboration

RESOURCE AVAILABILITY

Lead contact

Further information and requests for resources and reagents should be directed to and will be fulfilled by the lead contact, Eliza Loo (loo@hhu.de)

Materials availability

This study did not generate new unique reagents.

Data and code availability

Raw 16S sequencing data have been deposited into the European Nucleotide Archive (ENA) under the accession number PRJEB63568. In addition, the scripts used for the computational analyses described in this study are available at GitHub https://github.com/duranpa/sweet_collaboration. Raw metabolomics file is deposited at <https://www.metabolomicsworkbench.org> under the data track Study ID ST002779. Any additional information required to reanalyze the data reported in this paper is available from the [lead contact](#) upon request.

EXPERIMENTAL MODEL

Arabidopsis thaliana Col-0 seeds were sterilized in a 1.5-mL microcentrifuge tube with 1 mL of 30% chlorine + 0.1% Triton X-100 for 15–20 min at room temperature with agitation. The seeds were rinsed once with 1 mL of 80% ethanol, followed by five rinses with autoclaved ddH₂O. The microcentrifuge tube was wrapped in aluminum foil and cold-treated at 4 °C for 2–5 days before sowing. *A. thaliana* Col-0 seeds were incubated under standard growth conditions, i.e., 22 °C, 10 h light/ 14 h dark, 60% humidity, 180–230 $\mu\text{mol/s/m}^2$ light intensity.

CD-Rhizotron

To assemble a CD-Rhizotron, a small opening, measuring approximately 1.5–2 cm, was cut on the top of a slimline jewel CD case (14.3 cm x 12.4 cm x 0.52 cm; [Figure S1A](#)). The teeth of the tray were snipped off and sanded down to produce a smooth surface. The resulting hole was sealed on both sides with packing tape. CD-Rhizotrons were filled with soil (Cologne Agricultural Soil, CAS⁴²) and wrapped with aluminum foil to provide a dark environment for proper root growth ([Figures S1A–S1D](#)). Up to four sterilized *A. thaliana* Col-0 seeds were sown directly onto each CD-Rhizotron from the top aperture of the CD-Rhizotron. CD-Rhizotrons were incubated under standard growth conditions. After 5–7 days, germinated seedlings were removed to leave each CD-Rhizotron with a single seedling. Plants were grown for another 3 weeks before they were harvested for microbiota profiling. Preparation of SynCom was adapted from (Durán et al.⁸²). The 60-member SynCom was curated based on differences in 16S rRNA sequence with a 97% threshold. Briefly, bacterial strains ([Table S5](#)) were cultivated in 50% Tryptic Soy Broth (Sigma) for one week at 28 °C with shaking at 200 rpm. The bacterial cultures were pooled in equal ratio and centrifuged at 4000x g for 10 mins. The bacterial pellet was re-suspended in 10 mM MgCl₂ to remove residual media and bacteria-derived metabolites. The washing step was repeated three times. The washed bacterial suspension was adjusted to an OD₆₀₀ of 0.02 (10⁷ cells/mL) prior to inoculation onto sterile peat soil.

ArtSoil preparation

For the preparation of 10% autoclaved soil suspension, sieved CAS (to remove pebbles) was dissolved in deionized water and autoclaved three times before use. Live bacterial suspension was prepared by inoculating fresh CAS into 10% autoclaved soil suspension to achieve desired bacterial dilution.⁸³ Autoclaved half-strength Murashige-Skoog (½ MS) media including MES (Duchefa Biochemie) and supplemented with 1% agar was cooled to 40–45 °C before it was inoculated with live bacterial suspension. Approximately 50 mL of ArtSoil media was used for each 12 cm x 12 cm culture plate ([Figure S2B](#)). Sterilized *A. thaliana* Col-0 seeds were sown and germinated on ArtSoil, and incubated in a plant growth chamber for 4 weeks under standard growth conditions.

METHOD DETAILS

Construction of translational GUS reporter lines

Genomic fragments comprising the 5'-upstream region and the entire coding region of *SWEET1*, *SWEET4*, *SWEET5*, *SWEET7*, *SWEET8*, *SWEET10*, and *SWEET13* were amplified by PCR using wild-type *A. thaliana* Col-0 genomic DNA as a template (primers for each gene are listed in Key Resource Table). The amplified products of *SWEET4*, *SWEET5*, *SWEET7*, *SWEET8*, and *SWEET10* were cloned into promoterless GUSplus vector⁸¹ while *SWEET1* and *SWEET13* were cloned into pMDC163 using the Gateway cloning system. All constructs were confirmed by sequencing. Wild-type *A. thaliana* Col-0 were transformed by *Agrobacterium tumefaciens* harboring SWEET-GUS constructs using the floral dip method. Transgenic seedlings were selected on ½ MS media supplemented with 1% sucrose and 25 $\mu\text{g/mL}$ hygromycin. Transgenic *SWEET2-GUS*, *SWEET11-GUS*, *SWEET12-GUS* and *SWEET17-GUS* were previously reported in Chen et al.,²⁸ Chen et al.,³⁴ and Guo et al.⁸⁰

GUS histochemical staining

Three-week-old plants were carefully removed from ArtSoil and rinsed with 70% ethanol. Each plant was inserted into one well in a 12-well plate before 1 mL of GUS staining solution (10 mM EDTA, 50 mM phosphate buffer, 0.1% Triton X-100, 1 mM potassium ferrocyanide, 1 mM potassium ferricyanide, 2 mM X-Gluc, 20% methanol) was added into each well. The plate was subsequently incubated in the dark at 37 °C for 1 h (*SWEET1*, 2, 17) or 4 h (*SWEET4*, 7, 8, 11, 12, 13). Prior to imaging, plants were removed from GUS staining buffer and rinsed with 70% ethanol.

Root metabolite profiling

Approximately 25–35 sterilized *A. thaliana* Col-0 seeds were sown in a row on ArtSoil and grown for 3 weeks. After 3 weeks, both primary and lateral roots longer than 8 cm were harvested by slicing with a scalpel. The roots were segmented into 2-cm segments measuring 0–2, 2–4, and 4–6 cm from the root tip. Lateral roots that emerged from primary roots were removed, if present. The roots were rinsed in distilled water, and blotted dry on Whatman filter papers before they were weighed and kept in 1.5-ml microcentrifuge tubes, each containing 2 metal beads. The samples were flash-frozen in liquid nitrogen and stored at -80 °C until the extraction process. For metabolite extraction, 0.5 mL of chilled extraction buffer (2:5:2 ratio of ddH₂O: methanol: chloroform containing 5 μM ribitol as internal standard) was added into each root sample and mixed by vortex for 20 sec. Metal beads in the tubes were removed. Sample tubes were shaken on a rotary shaker for 30 mins at 4 °C. The samples were then centrifuged at 20,000 x g for 5 min at 4 °C. After

centrifugation, 0.5 ml of supernatant was carefully aspirated and transferred to a clean 1.5-ml microcentrifuge tube. Samples were stored at -80 °C until they were subjected to GC-MS. For GC-MS analysis 30 µl of sample were dried by vacuum centrifugation in glass inlet tubes. Dried samples were derivatized according to Gu⁸⁴ and Shim et al.⁸⁵ Raw data files were converted to the mzXML format using ProteoWizard⁸⁶ and to the NetCDF format via MetAlign⁸⁷ using default parameters. Deconvolution of mass spectra was conducted using the free deconvolution software AMDIS (Automated Mass Spectral Deconvolution and Identification System from NIST). Deconvoluted mass spectra were matched against the NIST14 Mass Spectral Library (<https://www.nist.gov/srd/nist-standard-reference-database-1a-v14>). Database matches with more than 70% were further compared with an in-house chemical standard library for compound annotation. Compounds, that could not be verified by the in-house library are named according to the matched compound class and the retention time. Extracted ion peaks were integrated using MassHunter Quantitative (v b08.00, Agilent Technologies). For relative quantification, all metabolite peak areas were normalized to fresh weight and the peak area of the internal standard ribitol (Sigma-Aldrich) to correct for technical error. Here, a GC-based system was employed for metabolomics, which may detect only the fraction of metabolites that can be vaporized. It may be useful for a more in-depth analysis to use LC-based systems to identify more metabolites and improve coverage.

Microbiota profiling

Roots of 3-weeks-old plants grown *via* the CD-Rhizotrons were cut into 2-cm segments as described in “Root metabolite profiling” (Figures S1E and S1F). Each root segment was manually separated from the surrounding soil leaving only tightly adhered soil particles. The roots were then placed in 15 mL centrifuge tubes filled with 10 mL of deionized sterile water and inverted ten times to further displace residual soil from the roots. To harvest the root (endospheric) fraction, the roots were transferred to clean centrifuge tubes filled with 10 mL of detergent (0.1% Triton X-100 diluted in 1x TE) and shaken for two minutes. The roots were then transferred into clean centrifuge tubes filled with 10 mL of 80% ethanol and shaken for 30 seconds. The same step was repeated but replacing 80% ethanol with 2% bleach. Finally, roots were rinsed three times with deionized sterile water before they were dried on sterile filter papers and flash-frozen in liquid nitrogen and stored at -80 °C until further processing. To harvest the rhizospheric fraction, the soil wash-offs were centrifuged at 3000 × g for 10 min. The supernatants were discarded and the pellets were resuspended and transferred to clean 2 mL screwcap tubes. The tubes were centrifuged at 3000 × g for 10 min, after which the supernatant was discarded, and the pellets were flash-frozen in liquid nitrogen and stored in -80 °C for further processing. The similar protocol was applied for harvesting the root fraction of plants grown on ArtSoil. For rhizospheric fraction of plants grown on ArtSoil, a clean scalpel was used to scrape approximately 0.5 cm (wide) of agar along the surface where the roots grew. The agar scraps in clean microcentrifuge tubes were flash-frozen and stored at -80 °C for further processing.

DNA extraction and library preparation

Total DNA was extracted from the aforementioned samples using the FastDNA™ SPIN Kit for Soil (MP Biomedicals, Solon, USA) or NucleoSpin Soil Mini kit for DNA from soil (Macherey-Nagel GmbH & Co. KG, Düren, Germany) following instructions from the manufacturers. DNA samples were eluted in 50 µL nuclease-free water and used for microbial community profiling. DNA samples were used in a two-step PCR amplification protocol. In the first step, V4-V7 (799F: AACMGGATTAGATACCKG; 1192R: ACGTCATCCCCACCTTCC) of the bacterial 16S rRNA, was amplified. Under a sterile hood, each sample was amplified in triplicate in a 25 µL reaction volume containing 2 U DFS-Taq DNA polymerase, 1 × incomplete buffer (Bioron GmbH, Ludwigshafen, Germany), 2 mM MgCl₂, 0.3% BSA, 0.2 mM dNTPs (Life technologies GmbH, Darmstadt, Germany) and 0.3 µM forward and reverse primers. PCR was performed using the following parameters: 94 °C/2 min, 94 °C/30 s, 55 °C/30 s, 72 °C/30 s, 72 °C/10 min for 25 cycles. Afterwards, single-stranded DNA and proteins were digested by adding 1 µL of Antarctic phosphatase, 1 µL Exonuclease I, and 2.44 µL Antarctic phosphatase buffer (New England BioLabs GmbH, Frankfurt, Germany) to 20 µL of the pooled PCR product. Samples were incubated at 37 °C for 30 min and enzymes were deactivated at 85 °C for 15 min. Samples were centrifuged for 10 min at 3,000 × g and 3 µL of this reaction were used for a second PCR, prepared in the same way as described above using the same protocol but with cycles reduced to 10 and with primers including barcodes and Illumina adapters.⁸⁸ PCR quality was controlled by loading 5 µL of each reaction on a 1% agarose gel and affirming that no band was detected within the negative control. Amplicon concentration was determined fluorescently (Quant-iT™ PicoGreen™, Invitrogen), and equivalent DNA amounts of each of the bar-coded amplicons were pooled in one library. Then, 80 µL of the pooled library was loaded in a 1.5% agarose gel and run for 2 h at 80 V. Subsequently, bands with a size of ~500 bp were cut out and purified using the QIAquick gel extraction kit (Qiagen, Hilden, Germany). The final library concentration was estimated fluorescently (Quantus™ Fluorometer, Promega). Paired-end Illumina sequencing was performed in-house using the MiSeq sequencer and custom sequencing primers at the Max Planck Institute for Plant Breeding Research.

QUANTIFICATION AND STATISTICAL ANALYSIS

Amplicon sequencing data analysis

Sequencing reads were demultiplexed using Qiime2 (qiime demux emp_paired⁸⁹), and merged using Flash2.⁹⁰ Reads were denoised and dereplicated using Dada2⁹¹ and remaining individual reads were denoted as ASVs. Chimeras were removed using Qiime2 (vsearch uchime-denovo). Taxonomic classification was done via the Qiime feature classifier using the silva_138 and sequences classified as mitochondrial or chloroplast were removed from the dataset. Remaining ASVs were included in count tables.

Bray-Curtis dissimilarities between samples were calculated normalized ASV tables and performed PCAs using the *cmdscale* function (vegan R package). To quantify the effects of genotype and root region we used a constrained PCoA using the *capscale* function (vegan R package). To quantify the contribution of different variables and their interactions to the variance in pairwise Bray-Curtis dissimilarities, we analysed the Bray-Curtis distance matrix between pairs of samples with 999 iterations of a permutation-based test (permutational multivariate analysis of variance (PERMANOVA), *adonis* function, vegan R package), and removed technical and batch effects, using the formula as follows: *Bray-curtis* ~ *VariableX* + *Condition(Technical_replicates + Biological_replicates)*. We further inspected the effects of the variables using a constrained PCoA using the *capscale* function (vegan R package). Sequencing data from the SynCom experiment was pre-processed similarly as natural community 16S rRNA data. Quality-filtered merged paired-end reads were aligned to a reference set of sequences extracted from the whole-genome assemblies of the 60 strains included in the SynCom using Rbec79 (v1.0.0). A count table that was employed for downstream analyses of diversity was generated in R (v4.0.3) with the R package *vegan* (v2.5–6). Scripts for microbiota analysis and data visualization can be found at https://github.com/duranpa/sweet_collaboration

ANOVA for differential enrichment of metabolites

We applied the python package *statsmodels*⁹² to perform two-way analysis of variance (ANOVA⁹³). For a particular metabolite, we collected its mass spectrometry relative response in the WT or in *sweet* knockouts (line: WT vs. SWEET), and at different segments of the root (region: 2cm vs. 4cm vs. 6cm vs. whole). We fit a model that decomposes the relative response of the metabolite as a combination of line-specific and region-specific factors; this model is described by the following string in the code: '*relativeResponse* ~ *Line* + *Region*' and calculates a *P*-value for *Line* and one for *Region*. Using the *P*-value cutoff of 0.05 for *Line* (and *Region*), we determined the relative response of the metabolite to change significantly with *Line* (*Region*) if *P* < 0.05.

Quantify metabolic activities using PAS

Pathway activity score (PAS) was introduced to quantify the activity of different metabolic pathways in single-cell transcriptomes.^{94,95} It is designed with a permutation test along with a *P*-value to examine whether the gene expression of a pathway at a particular cell cluster is significantly higher or lower than the sample average. Since we are working with bulk RNA-seq and not scRNA-seq in the current study, this algorithm is modified, and the permutation test is no longer suitable and discarded.

There are 3 sources for pathways used in our analysis. (A) we obtained the pathway data of *Arabidopsis* from PlantCyc⁹⁶ (link to the tables <https://pmn.plantcyc.org/organism-summary?object=ARA>, downloaded on 18-NOV-2022). Pathways with patterns 'glucos', 'galactos', 'fructos', 'xylos', 'sucros', or 'maltos' in their name are considered relevant to sugar metabolism. (B) we are also interested in the potential to convert sucrose coming from the phloem into different sugars for secretion at different root segments, and these pathways are not clearly defined in PlantCyc. Thus, we applied flux balanced analysis to define the pathways of relevant metabolic reactions. See section 'Flux balance analysis (FBA) to define pathways' for the details of the algorithm. Table S6 shows the genes involved in each pathway. (C) we also assign the SWEET and SUC genes to their own single-gene-pathway to facilitate our analysis. This means the gene SWEET1 is assigned to a new pathway 'SWEET1', and so on.

Brady et al. performed bulk transcriptomics on different segments of *Arabidopsis* root.¹¹ The experiment involved two replicate roots. In the published dataset, the 13 segments of root 1 are labeled as: *LCOLUMELLASB*, *L1SB*, *L2SB*, ..., *L11SB*, *L12SB*; the 12 segments of root 2 are labeled as: *Slice1JW*, *Slice2JW*, ..., *Slice11JW*, *Slice12JW*. We found that the two roots are in different developmental stages, therefore we dropped root 2 and used only root 1 in our analysis.

Given the matrix of gene expression across different samples, we normalized the data using trimmed mean of M values (TMM) normalization.⁹⁷ In practice, this is implemented by the function *calcNormFactors* within the R package *edgeR*.⁹⁸ We used the function argument *method*="TMM" to call TMM and set *logratioTrim*=0.3.

Let us denote $g_{i,j}$ to be the normalized read count of gene *i* in sample *j*. The read count of a gene is normalized to give the relative transcript level, which is 1 when averaged over different samples. Mathematically, the relative transcript level of gene *i* at sample *j* is denoted as $r_{i,j}$, and is defined as $r_{i,j} = g_{i,j} / \left(\frac{1}{N} \sum_k g_{i,k} \right)$, where *N* is the total number of samples, and the label *k* goes over all samples.

The PAS of pathway *t* at sample *j* is denoted as $p_{t,j}$, which is a weighted average of the relative transcript levels across the genes of the pathway: $p_{t,j} = \sum_{i=1}^{m_t} w_i r_{i,j} / \sum_{i=1}^{m_t} w_i$. Here m_t is the number of genes in pathway *t*, and w_i is the weight of gene *i*, defined as the reciprocal of the number of pathways that gene *i* is involved in. Because $r_{i,j}$ is centered around 1, so do $p_{t,j}$. Thus, if $p_{t,j} > 1$, the expression of genes associated with pathway *t* in sample *j* is higher than the average over all samples, and vice versa.

Flux balance analysis (FBA) to define pathways

As we suspect that the root may convert sucrose into other sugars before secretion, we would like to find out the genes involved in these conversion pathways for further analysis. To assign genes in the metabolic network to these pathways, we applied FBA,⁹⁹ which searches for the combination of genes and reactions that results in the highest yield for such conversions, assuming sucrose to be the sole input carbon source of the metabolic network.

We used the AraGEM¹⁰⁰ a curated FBA model of *Arabidopsis*, to perform our simulations and define the genes associated with each conversion pathway. The AraGEM model is published with 3 different sets of parameters that correspond to their own case of metabolism: (a) photosynthesis, (b) photorespiration, and (c) non-photosynthetic cell. Case (c) is relevant to the root condition,

as it considers the conversion of sucrose into other biomass metabolites. Hence, our simulations are developed from case (c), which uses sucrose as the input carbon source.

We switched off the default objective function of AraGEM, which includes a set of metabolites with weights found in real plants. To investigate the conversion of sucrose into different sugars, we set different monosaccharides, disaccharides and combinations of monosaccharides as the objective; these include all possible monosaccharides and disaccharides in AraGEM. In total, we analyzed 11 different objective functions: (1) maltose, (2) glucose, (3) beta-D-fructose, (4) D-galactose, (5) D-xylose, (6) glucose + beta-D-fructose, (7) glucose + D-galactose, (8) glucose + D-xylose, (9) beta-D-fructose + D-galactose, (10) beta-D-fructose + D-xylose, (11) D-galactose + D-xylose. Note that the molecules within objective functions have equal weights, as some of them have multiple sugar molecules.

We used the python package COBRApy¹⁰¹ along with the GUROBI solver (Gurobi Optimizer Version 3.0. Houston, Texas: Gurobi Optimization, Inc., April 2010. (software program)) to perform FBA simulation. For each of the 11 objective functions, we performed parsimony-FBA simulation¹⁰² to find out the most efficient reactions that perform the conversion of sucrose into the objective sugars. We also calculated the shadow price¹⁰³ of each metabolite involved in these reactions; a metabolite with negative shadow price is deemed critical, as an extra supply of this metabolite leads to a higher flux of the objective function. Reactions that have critical metabolites both at their input and output are also considered critical. We collected all the critical reactions of an objective function, and the genes associated with any critical reactions are assigned to the pathway (refer to [Table S6](#) for the genes in these pathways).

Correlation between microbes and metabolites

We calculated the correlation between every pair of microbes and metabolites to reveal the potential cross feeding between the microbe species. At each combination of plant lineages (WT / SWEET2 / SWEET4 / SWEET11,22) and root segments (2cm / 4cm / 6cm / whole root), we performed 16s RNA sequencing to quantify the abundance of different microbial classes and also mass spectrometry to measure the abundance of different metabolites.

For each pair of microbe class and metabolite, we calculated their spearman correlation across different plant lineages and root locations to construct the correlation matrix; matrix elements that correspond to p-value >0.05 are deemed insignificant and replaced with 0 (i.e., not connected in a complex network). We used the iGraph package of R to display this bipartite network.¹⁰⁴ Communities within this network are detected using the label propagation algorithm.¹⁰⁵

Reference ID: KRT64abe6afd69ae

Cell Host & Microbe, Volume 32

Supplemental information

**Sugar transporters spatially organize microbiota
colonization along the longitudinal
root axis of *Arabidopsis***

Eliza P.-I. Loo, Paloma Durán, Tin Yau Pang, Philipp Westhoff, Chen Deng, Carlos Durán, Martin Lercher, Ruben Garrido-Oter, and Wolf B. Frommer

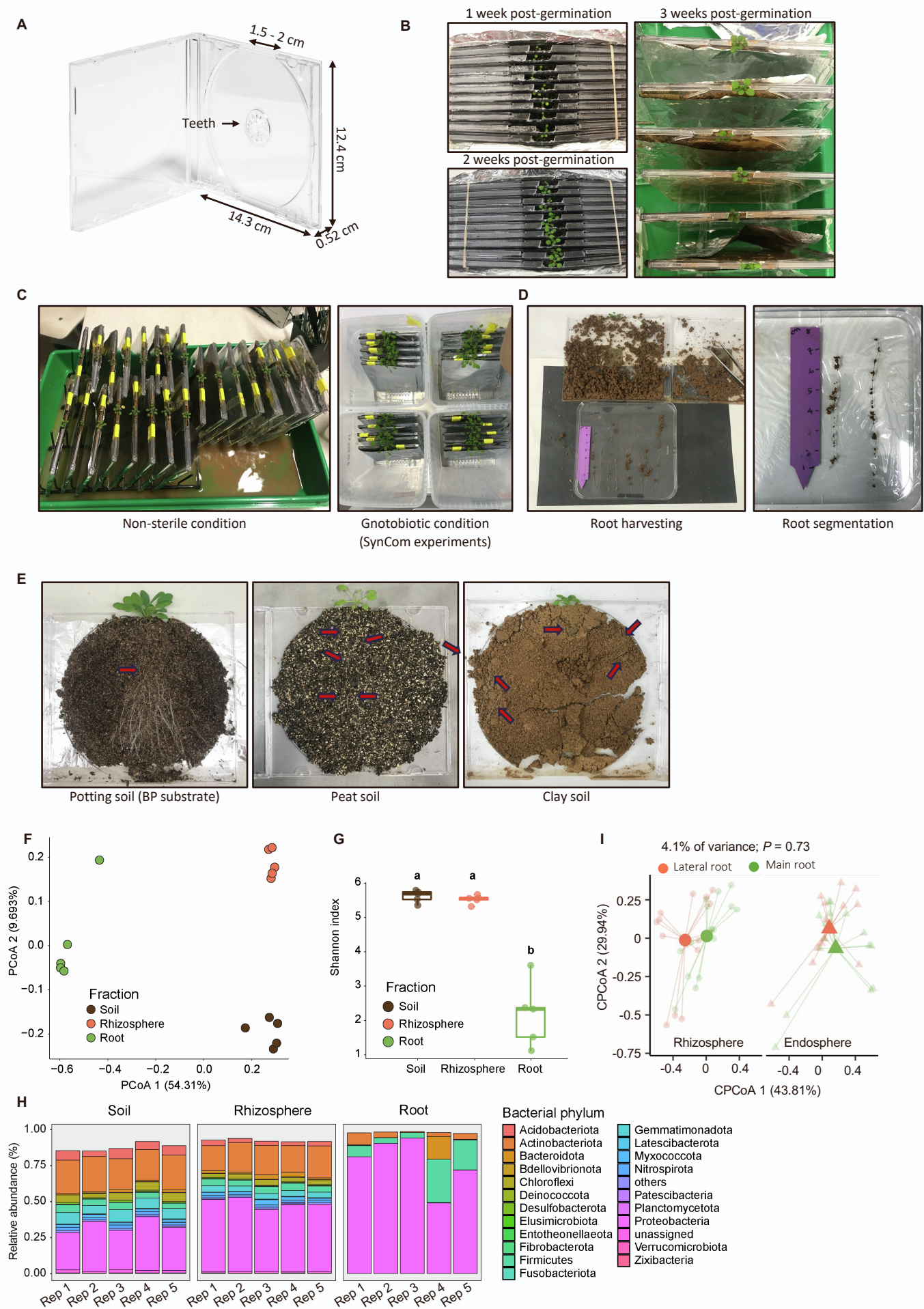


Figure S1: Development of CD-Rhizotron to study spatial colonization of root bacteria (related to Figure 1 and STAR Methods)

- A) Construction of CD-Rhizotron, with dimensions indicated.
- B) Phenotype of *A. thaliana* plants grown *via* CD-Rhizotron at different growth stages. Sterilized *A. thaliana* seeds were sown directly on the soil through the top opening. CD-Rhizotron was wrapped with aluminium foil to ensure root growth in darkness.
- C) Growth set-up for *A. thaliana* seedlings *via* CD-Rhizotron for non-sterile and gnotobiotic SynCom (CD-Rhizotron grown in sterile microboxes) experiments.
- D) Process of harvesting roots from CD-Rhizotron and the resulting roots harvested for subsequent sectioning and microbiota profiling.
- E) Growth of *A. thaliana* on different soil types in CD-Rhizotron. Examples of individual strands of root (except for potting soil) indicated with arrows.
- F) Bray-Curtis dissimilarity analysis of root bacterial community from *A. thaliana* grown *via* CD-Rhizotron. The fraction ‘soil’ refers to bacterial communities derived from bulk soil without the presence of plants, ‘rhizosphere’ refers to bacterial communities derived from soil tightly attached to roots, ‘endosphere’ refers to bacterial communities derived from root tissues.
- G) Shannon diversity of root bacterial community from *A. thaliana* grown *via* CD-Rhizotron.
- H) Relative abundance of root bacterial community from *A. thaliana* grown *via* CD-Rhizotron. ASVs with relative abundance <0.5% were filtered. Each bar represents the average relative abundance of biological replicates from 5 independent experiments.
- I) Bray-Curtis dissimilarity analysis of endospheric and rhizospheric bacterial community derived from lateral and main roots of *A. thaliana* grown on CD-Rhizotron.

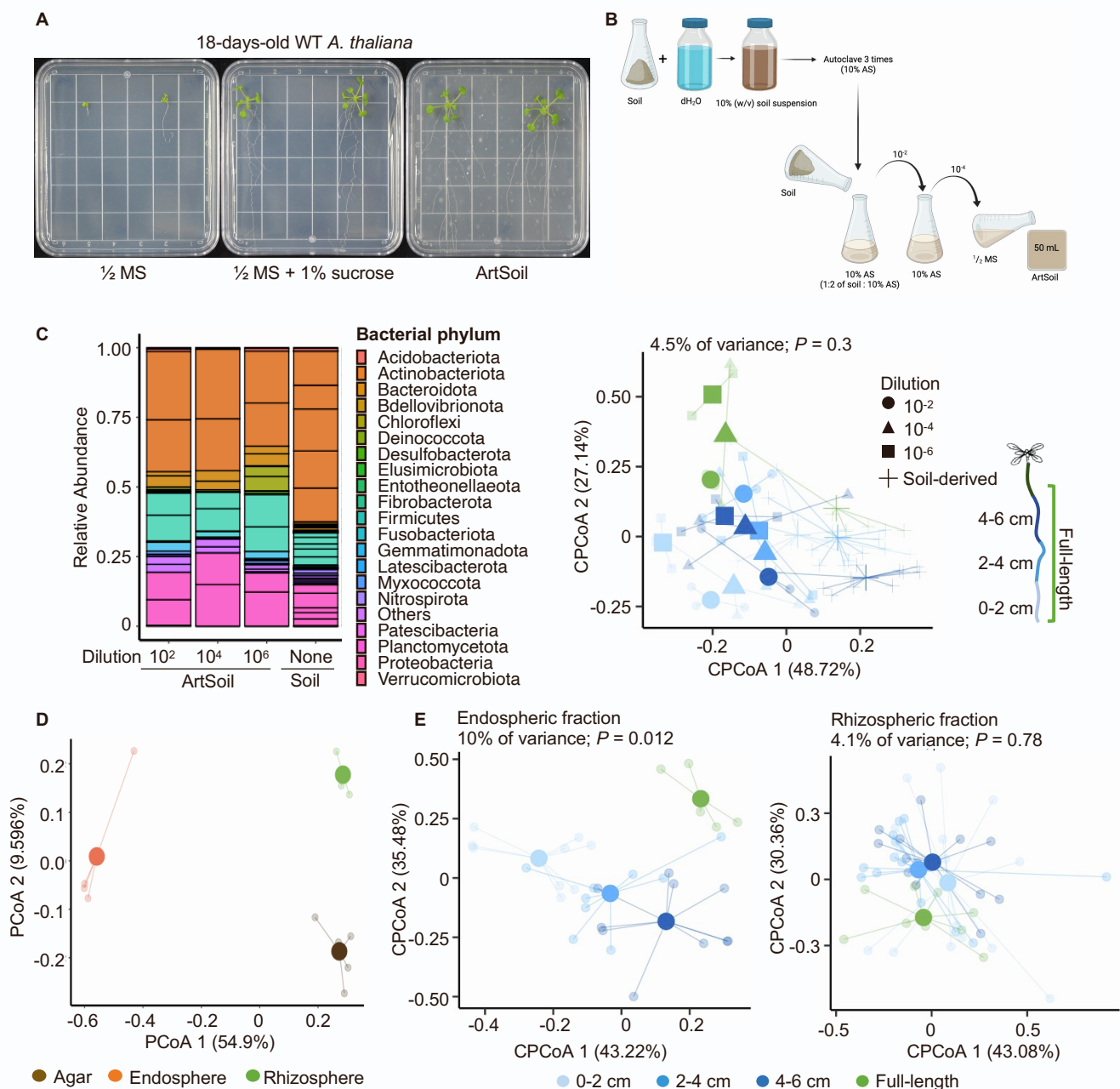


Figure S2: ArtSoil- a simple-to-assemble plant growth system for soil-like growth conditions (related to Figure 1 and STAR Methods)

- A) Phenotype of *A. thaliana* seedlings grown on $\frac{1}{2}$ MS-salt, $\frac{1}{2}$ MS-salt supplemented with 1% sucrose, and ArtSoil.
- B) Step-by-step illustration for the preparation of ArtSoil. AS- Autoclave soil suspension. Image created with Biorender.
- C) Relative abundance and Bray-Curtis dissimilarity analysis of endospheric bacterial community derived from roots of soil-grown *A. thaliana* or plants grown on ArtSoil with 10^{-2} , 10^{-4} , and 10^{-6} dilutions of soil.
- D) Bray-Curtis dissimilarity analysis of root bacterial community from *A. thaliana* grown on ArtSoil. The fraction ‘agar’ refers to bacterial communities derived from bulk agar containing soil suspension without the presence of plants, ‘rhizosphere’ refers to bacterial communities derived from soil tightly attached to roots, ‘endosphere’ refers to bacterial communities derived from root tissues.
- E) Bray-Curtis dissimilarity analysis of root bacterial community from *A. thaliana* grown in soil inoculated with SynCom. The fraction ‘0-2 cm’, ‘2-4 cm’, and ‘4-6 cm’ refers to bacterial communities derived from indicated locations of the root, ‘full-length’ refers to bacterial communities derived from the entire length of the root.

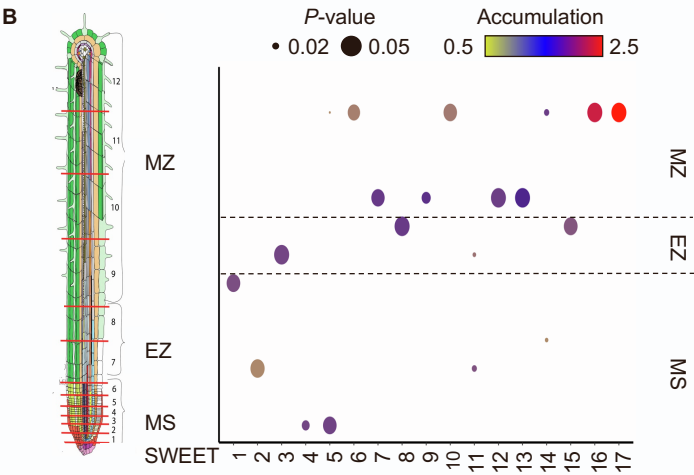
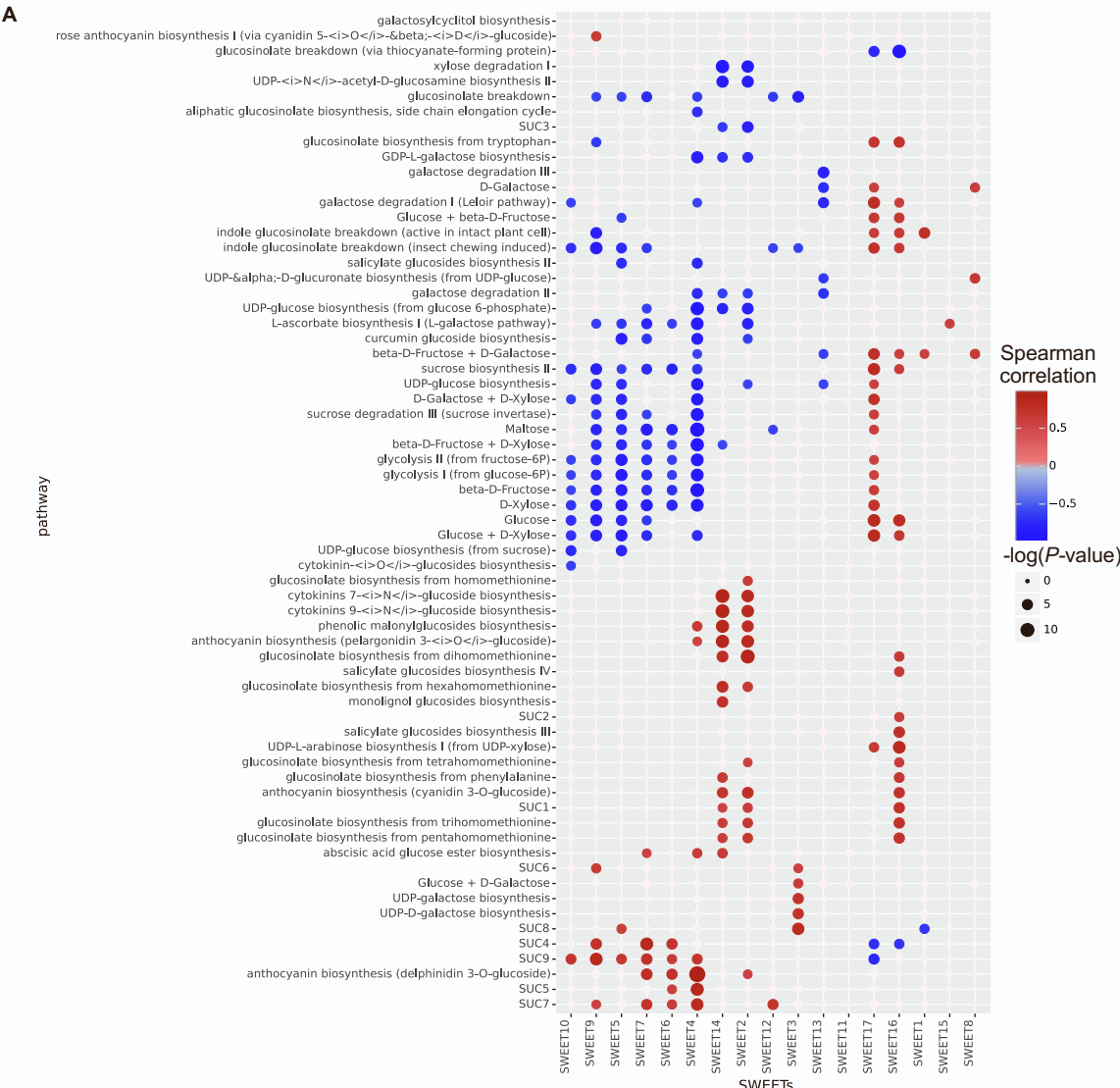


Figure S3: Bioinformatics prediction of *SWEETs*' involvement in root sugar metabolic pathways (related to Figure 2)

- A) Correlation between each member of *SWEET* and sugar-related metabolic pathway in the root. Color indicates positive or negative correlation between each *SWEET* with a particular metabolic pathway; size of circle indicates statistical significance of the correlation.
- B) Average accumulation of respective *SWEET* mRNA transcripts along the root axis. MS- meristematic zone (<0.25 mm), EZ- elongation zone (0.25-0.5 mm), MZ- maturation zone (>0.5 mm). Color indicates the relative amount of mRNA accumulation; the size of circle indicates statistical significance of the mRNA accumulation in indicated root zones.

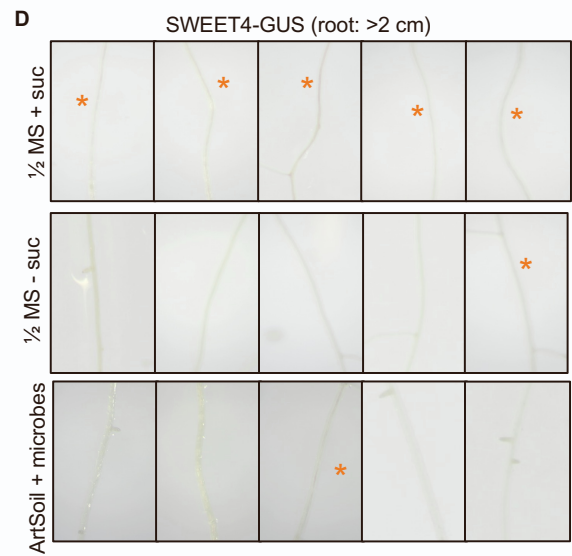
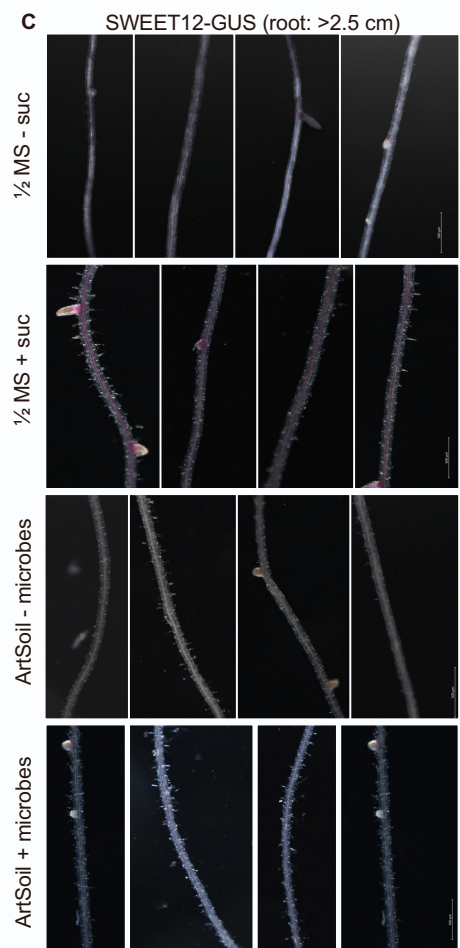
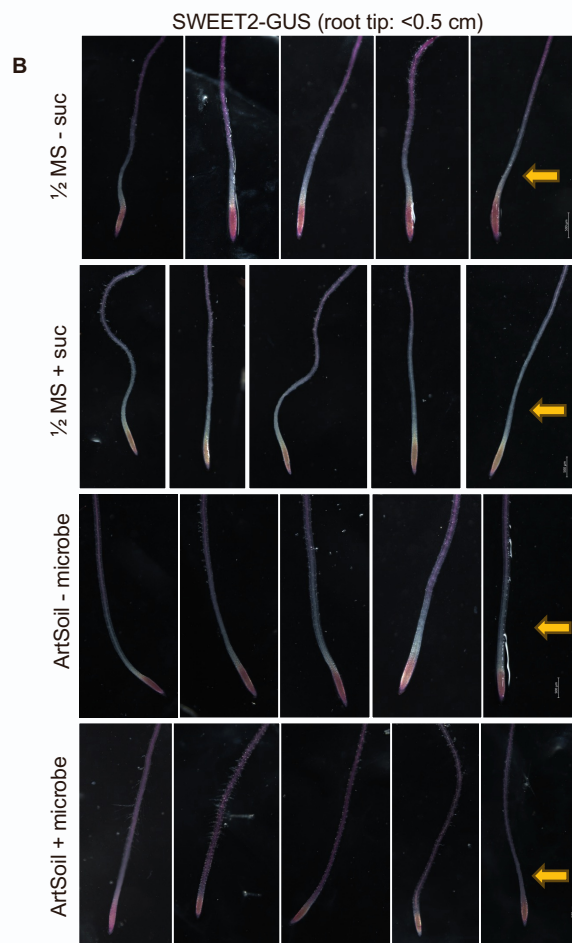
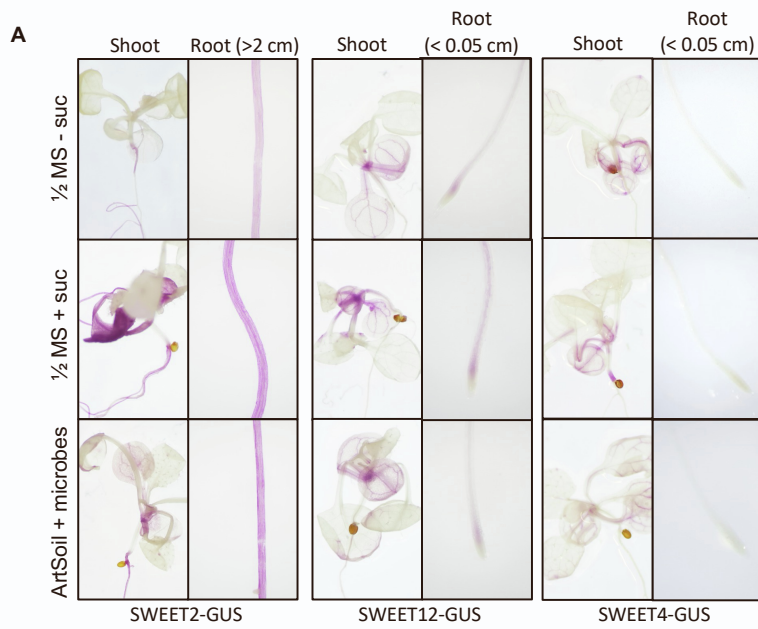


Figure S4: Accumulation of SWEET2-GUS, SWEET12-GUS, and SWEET4-GUS in plants grown on $\frac{1}{2}$ MS \pm suc or ArtSoil with heat-killed or live microbes (related to Figure 3)

- A) Unaltered spatial accumulation of SWEET2-GUS, SWEET12-GUS and SWEET4-GUS in the shoot and indicated regions of the root in plants grown on indicated media. Representative image from $N > 10$. Individual images are shown in Figure S4B-D.
- B) Accumulation of SWEET2-GUS in the region just above the root tip (<0.05 cm) is observed only in plants grown ArtSoil with live microbes. Yellow arrows indicate the (accumulation) zone of interest. Scale bar: 500 μ m.
- C) Accumulation of SWEET12-GUS in the regions above 2 cm from the root tip is observed in the vasculature of plants grown on $\frac{1}{2}$ MS + suc and ArtSoil with live microbes. Scale bar: 500 μ m.
- D) Patchy accumulation of SWEET4-GUS in the regions above 2 cm from the root tip is observed only in plants grown on $\frac{1}{2}$ MS + suc. Scale bar: 500 μ m. $\frac{1}{2}$ MS - suc: $\frac{1}{2}$ MS media without sucrose supplementation, $\frac{1}{2}$ MS + suc: $\frac{1}{2}$ MS media with sucrose supplementation, ArtSoil - microbes: ArtSoil inoculated with heat-killed soil microbes, ArtSoil + microbes: ArtSoil inoculated with soil microbes. All experiments above were repeated at least 3 times, each time $N > 6$.

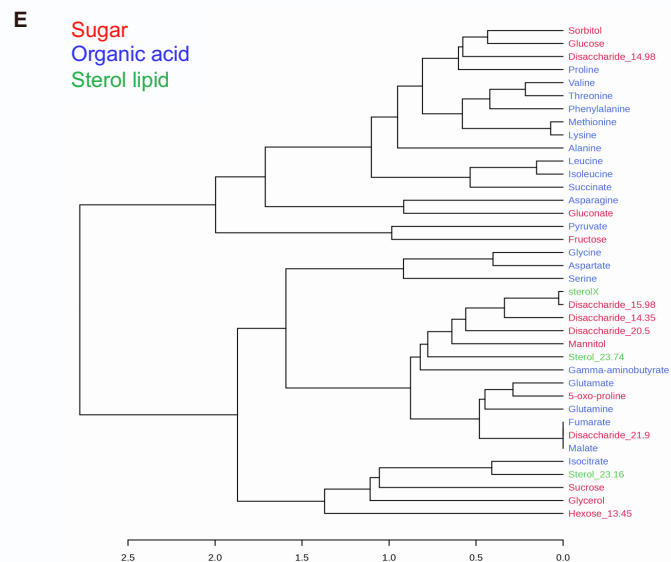
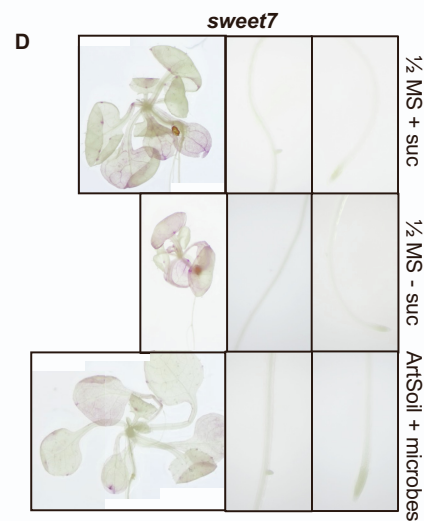
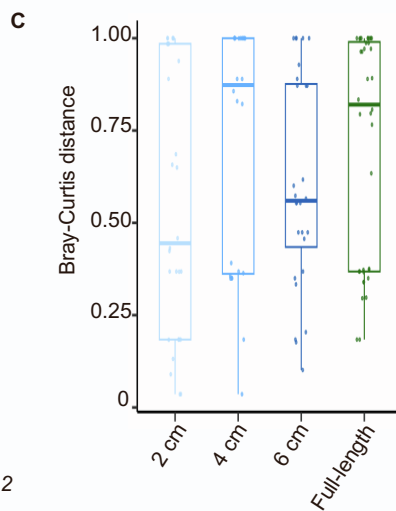
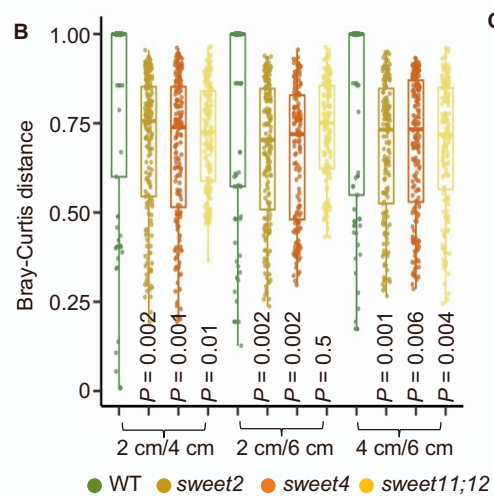
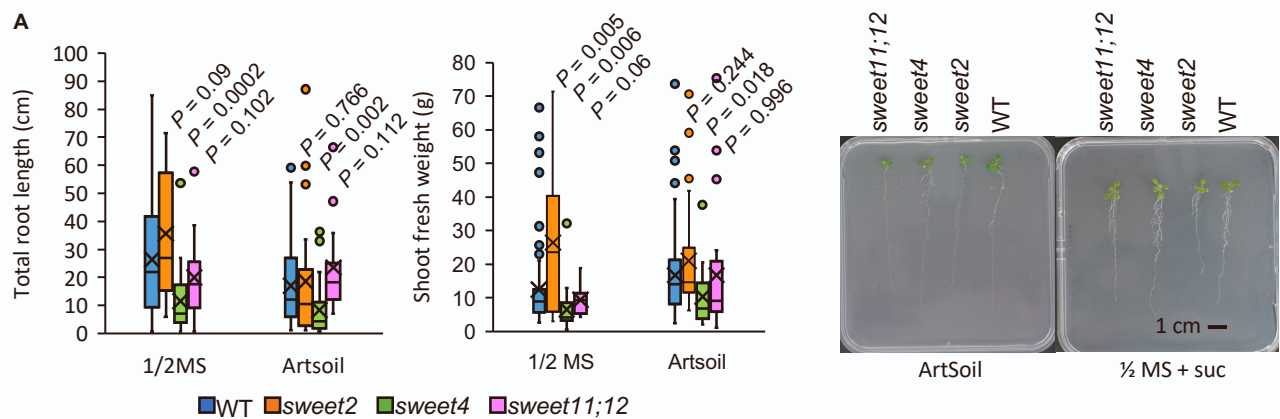


Figure S5: Phenotypes, spatial metabolite and microbiota profiles of *sweet* knock-out lines (related to Figures 4 and 5)

- A) Total root length and shoot fresh weight of WT, *sweet2*, *sweet4*, and *sweet11;12* knock-out lines grown on $\frac{1}{2}$ MS or ArtSoil + microbes. *P*-values were calculated using Welch's ANOVA. The experiment was repeated twice, $N > 20$.
- B) Pairwise comparison between Bray-Curtis distances of root microbiota derived from root segments of each genotype. X-axis indicates the root segments compared. Colors indicate plant genotype. *P*-values (Student's t-test) for *sweets* calculated against WT plants. See also Tables S1-S3.
- C) Bray-Curtis dissimilarities distances of root microbiota derived from each root segment compared to the full-length root of *sweet7* knock-out plants. Different colors represent respective root segments or full-length root samples as depicted in the cartoon on the left.
- D) Histochemical staining of SWEET7-GUS seedlings grown on $\frac{1}{2}$ MS-salt \pm suc or ArtSoil + microbes. $N > 10$.
- E) Dendrogram depicting ranking of metabolite correlation with microbes (at class level) based on Spearman average linkage hierarchical clustering. Colors indicate classes of metabolites.

Table S1: Statistical analyses for beta-diversity analyses. *P*-values calculated using PERMANOVA (related to Figure 1 and Figure 5B)

Root segment pair	Corresponding figure	<i>P</i> -value
WT: 2 cm vs 4 cm	Figure 1A (Endosphere)	0.005
WT: 2 cm vs 6 cm	Figure 1A (Endosphere)	0.002
WT: 4 cm vs 6 cm	Figure 1A (Endosphere)	0.007
WT: 2 cm vs 4 cm	Figure 1A (Rhizosphere)	0.015
WT: 2 cm vs 6 cm	Figure 1A (Rhizosphere)	0.037
WT: 4 cm vs 6 cm	Figure 1A (Rhizosphere)	0.007
WT: 2 cm vs 4 cm	Figure 1B (Endosphere)	0.01
WT: 2 cm vs 6 cm	Figure 1B (Endosphere)	0.05
WT: 4 cm vs 6 cm	Figure 1B (Endosphere)	0.2
WT: 2 cm vs 4 cm	Figure 1B (Rhizosphere)	0.24
WT: 2 cm vs 6 cm	Figure 1B (Rhizosphere)	0.69
WT: 4 cm vs 6 cm	Figure 1B (Rhizosphere)	0.72
sweet2: 2 cm vs 4 cm	Figure 5B	0.67
sweet2: 2 cm vs 6 cm	Figure 5B	0.2
sweet2: 4 cm vs 6 cm	Figure 5B	0.65
sweet4: 2 cm vs 4 cm	Figure 5B	0.2
sweet4: 2 cm vs 6 cm	Figure 5B	0.04
sweet4: 4 cm vs 6 cm	Figure 5B	0.6
sweet11;12: 2 cm vs 4 cm	Figure 5B	0.003
sweet11;12: 2 cm vs 6 cm	Figure 5B	0.05
sweet11;12: 4 cm vs 6 cm	Figure 5B	0.04
2 cm: WT vs sweet2	Figure 5B	0.6
2 cm: WT vs sweet4	Figure 5B	0.7
2 cm: WT vs sweet11/12	Figure 5B	0.05
2 cm: sweet2 vs sweet4	Figure 5B	0.5
2 cm: sweet2 vs sweet11/12	Figure 5B	0.02
2 cm: sweet4 vs sweet11/12	Figure 5B	0.02
4 cm: WT vs sweet2	Figure 5B	0.3
4 cm: WT vs sweet4	Figure 5B	0.01
4 cm: WT vs sweet11/12	Figure 5B	0.3
4 cm: sweet2 vs sweet4	Figure 5B	0.11
4 cm: sweet2 vs sweet11/12	Figure 5B	0.46
4 cm: sweet4 vs sweet11/12	Figure 5B	0.1
6 cm: WT vs sweet2	Figure 5B	0.8
6 cm: WT vs sweet4	Figure 5B	0.8
6 cm: WT vs sweet11/12	Figure 5B	0.9
6 cm: sweet2 vs sweet4	Figure 5B	0.18
6 cm: sweet2 vs sweet11/12	Figure 5B	0.12
6 cm: sweet4 vs sweet11/12	Figure 5B	0.41

Table S2: Bray-Curtis distance of each root segment for each genotype (Related to Figure 5B)

Root segment 1	Root segment 2	Mean Bray-Curtis distance	Standard error
2 cm WT	4 cm WT	0.814	0.033
2 cm WT	6 cm WT	0.761	0.032
4 cm WT	6 cm WT	0.798	0.031
2 cm <i>sweet11/12</i>	2 cm <i>sweet11/12</i>	0.742	0.012
2 cm <i>sweet11/12</i>	4 cm <i>sweet11/12</i>	0.713	0.011
2 cm <i>sweet11/12</i>	6 cm <i>sweet11/12</i>	0.729	0.011
4 cm <i>sweet11/12</i>	6 cm <i>sweet11/12</i>	0.688	0.014
2 cm <i>sweet2</i>	6 cm <i>sweet2</i>	0.69	0.015
2 cm <i>sweet2</i>	4 cm <i>sweet2</i>	0.671	0.015
4 cm <i>sweet2</i>	6 cm <i>sweet2</i>	0.676	0.015
2 cm <i>sweet4</i>	4 cm <i>sweet4</i>	0.676	0.016
2 cm <i>sweet4</i>	6 cm <i>sweet4</i>	0.665	0.015
4 cm <i>sweet4</i>	4 cm <i>sweet4</i>	0.692	0.014

Table S3: Statistical analyses on pairwise comparison of Bray-Curtis distances between root segments of each genotype (Related to Figure 5B)

Root segment pair 1	Root segment pair 2	N pair 1	N pair 2	Test statistic	Degree of freedom	p	p.adj	p.adj.signif
2 cm WT vs. 4 cm WT	2 cm <i>sweet11/12</i> vs. 4 cm <i>sweet11/12</i>	81	169	2.864735846	98.2315757	0.005	0.010	**
2 cm WT vs. 4 cm WT	2 cm <i>sweet11/12</i> vs. 6 cm <i>sweet11/12</i>	81	169	2.441034521	97.18186883	0.016	0.029	*
2 cm WT vs. 4 cm WT	2 cm <i>sweet2</i> vs. 4 cm <i>sweet2</i>	81	182	3.40435836	113.0133652	0.001	0.002	**
2 cm WT vs. 4 cm WT	2 cm <i>sweet2</i> vs. 6 cm <i>sweet2</i>	81	182	3.920134494	112.6121207	0.000	0.000	***
2 cm WT vs. 4 cm WT	2 cm <i>sweet4</i> vs. 4 cm <i>sweet4</i>	81	168	3.735804971	117.5454259	0.000	0.001	***
2 cm WT vs. 4 cm WT	2 cm <i>sweet4</i> vs. 6 cm <i>sweet4</i>	81	156	4.063475204	113.4537742	0.000	0.000	***
2 cm WT vs. 4 cm WT	4 cm <i>sweet11/12</i> vs. 2 cm <i>sweet11/12</i>	81	169	2.864735846	98.2315757	0.005	0.010	**
2 cm WT vs. 4 cm WT	4 cm <i>sweet11/12</i> vs. 6 cm <i>sweet11/12</i>	81	169	3.504299554	108.3338739	0.001	0.001	**
2 cm WT vs. 4 cm WT	4 cm <i>sweet2</i> vs. 6 cm <i>sweet2</i>	81	169	3.76172002	113.4357328	0.000	0.001	***
2 cm WT vs. 4 cm WT	4 cm <i>sweet4</i> vs. 6 cm <i>sweet4</i>	81	182	3.364632907	110.6614455	0.001	0.002	**
2 cm WT vs. 6 cm WT	2 cm <i>sweet11/12</i> vs. 4 cm <i>sweet11/12</i>	81	169	1.382449213	99.56724944	0.170	0.248	ns
2 cm WT vs. 6 cm WT	2 cm <i>sweet11/12</i> vs. 6 cm <i>sweet11/12</i>	81	169	0.941018543	98.44033626	0.349	0.456	ns
2 cm WT vs. 6 cm WT	2 cm <i>sweet2</i> vs. 4 cm <i>sweet2</i>	81	182	1.992994247	115.4339219	0.049	0.082	ns
2 cm WT vs. 6 cm WT	2 cm <i>sweet2</i> vs. 6 cm <i>sweet2</i>	81	182	2.522507494	115.0038529	0.013	0.024	*
2 cm WT vs. 6 cm WT	2 cm <i>sweet4</i> vs. 4 cm <i>sweet4</i>	81	168	2.349954042	120.2662808	0.020	0.036	*
2 cm WT vs. 6 cm WT	2 cm <i>sweet4</i> vs. 6 cm <i>sweet4</i>	81	156	2.673995089	115.8720671	0.009	0.017	*
2 cm WT vs. 6 cm WT	4 cm <i>sweet11/12</i> vs. 2 cm <i>sweet11/12</i>	81	169	1.382449213	99.56724944	0.170	0.248	ns
2 cm WT vs. 6 cm WT	4 cm <i>sweet11/12</i> vs. 6 cm <i>sweet11/12</i>	81	169	2.079938776	110.4055996	0.040	0.068	ns
2 cm WT vs. 6 cm WT	4 cm <i>sweet2</i> vs. 6 cm <i>sweet2</i>	81	169	2.362761347	115.8711254	0.020	0.036	*
2 cm WT vs. 6 cm WT	4 cm <i>sweet4</i> vs. 6 cm <i>sweet4</i>	81	182	1.943936991	112.912498	0.054	0.089	ns
4 cm WT vs. 6 cm WT	4 cm <i>sweet11/12</i> vs. 2 cm <i>sweet11/12</i>	81	169	2.552494521	101.2373283	0.012	0.022	*
4 cm WT vs. 6 cm WT	4 cm <i>sweet11/12</i> vs. 6 cm <i>sweet11/12</i>	81	169	3.237768258	112.9913376	0.002	0.004	**
4 cm WT vs. 6 cm WT	4 cm <i>sweet2</i> vs. 6 cm <i>sweet2</i>	81	169	3.512329433	118.9060431	0.001	0.001	**
4 cm WT vs. 6 cm WT	4 cm <i>sweet4</i> vs. 6 cm <i>sweet4</i>	81	182	3.089418103	115.7231696	0.003	0.006	**

Table S4: Metabolites and their retention times identified from root tissues using untargeted GC/MS (related to Figure 2)

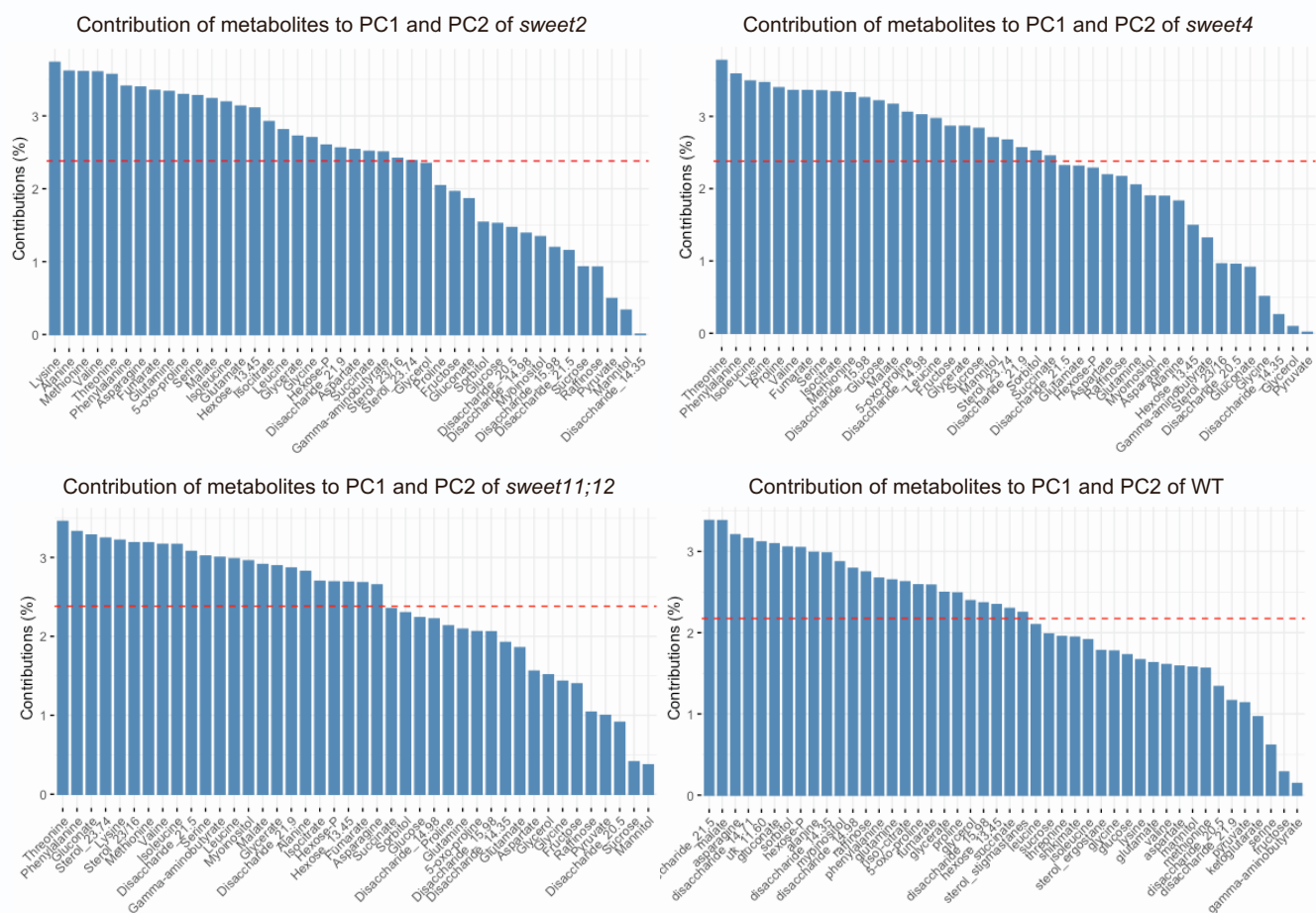
Metabolite	Superclass (MetFR)	Subclass (according to the Human Metabolome Database)	mass/fragment	Retention time (s)
Sterol_23.74	Sterol Lipids	Stigmastanes and derivatives	396	23.74
5-oxo-proline	Carbohydrates	Carbohydrates and carbohydrate conjugates	156.1	11.172
Alanine	Organic acids	Amino acids, peptides, and analogues	116.09	6.618
Ketoglutarate	Organic acids	Dicarboxylic acids and derivatives	198.06	11.668
Asparagine	Organic acids	Amino acids, peptides, and analogues	116.085	12.579
Aspartate	Organic acids	Amino acids, peptides, and analogues	232.119	11.155
Sterol_23.16	Sterol Lipids	Ergostane steroids	382	23.16
Isocitrate	Organic acids	Tricarboxylic acids and derivatives	273.098	13.925
Dimethylolpropanoic acid	(Internal standard)	(Internal standard)	148	11.668
Fructose	Carbohydrates	Carbohydrates and carbohydrate conjugates	307	14.444
Fumarate	Organic acids	Dicarboxylic acids and derivatives	245.067	9.28
Gamma-aminobutyrate	Organic acids	Amino acids, peptides, and analogues	304.1	11.233
Disaccharide_21.9	Carbohydrates	Carbohydrates and carbohydrate conjugates	204	21.9
Hexose	Carbohydrates	Carbohydrates and carbohydrate conjugates	387	17.8
Gluconate	Carbohydrates	Carbohydrates and carbohydrate conjugates	333.138	15.42
Glucose	Carbohydrates	Carbohydrates and carbohydrate conjugates	205.108	14.663
Glutamate	Organic acids	Amino acids, peptides, and analogues	246.135	12.09
Glutamine	Organic acids	Amino acids, peptides, and analogues	156.1	13.45
Glycerate	Carbohydrates	Carbohydrates and carbohydrate conjugates	189.077	9.189
Glycerol	Carbohydrates	Carbohydrates and carbohydrate conjugates	205.108	8.561
Glycine	Organic acids	Amino acids, peptides, and analogues	174.113	8.926
Isoleucine	Organic acids	Amino acids, peptides, and analogues	158.137	8.774
Disaccharide_21.5	Carbohydrates	Carbohydrates and carbohydrate conjugates	204	21.5
Disaccharide_14.71	Carbohydrates	Carbohydrates and carbohydrate conjugates	204	14.716
Leucine	Organic acids	Amino acids, peptides, and analogues	158.137	8.527
Lysine	Organic acids	Amino acids, peptides, and analogues	174.113	14.714
Malate	Organic acids	Dicarboxylic acids and derivatives	233.103	10.835
Disaccharide_20.5	Carbohydrates	Carbohydrates and carbohydrate conjugates	361.169	20.515
Mannitol	Carbohydrates	Monosaccharide	205.108	14.927
Disaccharide_14.98	Carbohydrates	Carbohydrates and carbohydrate conjugates	217	14.98
Methionine	Organic acids	Amino acids, peptides, and analogues	176.093	11.135
Myoinositol	Carbohydrates	Monosaccharide	305.1425	16.158
Phenylalanine	Organic acids	Amino acids, peptides, and analogues	192.12	12.181
Proline	Organic acids	Amino acids, peptides, and analogues	142.1	8.818
Pyruvate	Organic acids	Alpha-keto acids and derivatives	174.0586	6.025
Raffinose	Carbohydrates	Carbohydrates and carbohydrate conjugates	437.203	24.574
Ribitol	(Internal standard)	(Internal standard)	217	13.165
Serine	Organic acids	Amino acids, peptides, and analogues	204.124	9.509
Shikimate	Organic oxygen compounds	Alcohols and polyols	204.1	13.783
Sorbitol	Carbohydrates	Monosaccharide	319.158	14.991
Succinate	Organic acids	Dicarboxylic acids and derivatives	247.082	8.939
Sucrose	Carbohydrates	Carbohydrates and carbohydrate conjugates	361.169	19.886
Hexose_13.45	Carbohydrates	Carbohydrates and carbohydrate conjugates	217	13.45
Uk_11.60	Carbohydrates	Carbohydrates and carbohydrate conjugates	292.1	11.671
Threonine	Organic acids	Amino acids, peptides, and analogues	219.11	9.806
Disaccharide_14.35	Carbohydrates	Carbohydrates and carbohydrate conjugates	361	14.354
Disaccharide_15.98	Carbohydrates	Carbohydrates and carbohydrate conjugates	361	15.98
Valine	Organic acids	Amino acids, peptides, and analogues	144.121	7.91

Table S5: Information for members of Syncom used in this study (related to STAR Methods)

Syncom member ID	Kingdom	Phylum	Class	Order	Family	Genus
Root151	Bacteria	Actinobacteria	Actinobacteria	Actinomycetales	Nocardioidaceae	Nocardioides
Root562	Bacteria	Proteobacteria	Gammaproteobacteria	Pseudomonadales	Pseudomonadaceae	Pseudomonas
Root61	Bacteria	Proteobacteria	Gammaproteobacteria	Xanthomonadales	Xanthomonadaceae	Rhodanobacter
Root136	Bacteria	Actinobacteria	Actinobacteria	Actinomycetales	Nocardiaceae	Nocardia
Root123D2	Bacteria	Proteobacteria	Alphaproteobacteria	Rhizobiales	Bradyrhizobiaceae	Afipia
Root1298	Bacteria	Proteobacteria	Alphaproteobacteria	Rhizobiales	Rhizobiaceae	Rhizobium
Root672	Bacteria	Proteobacteria	Alphaproteobacteria	Sphingomonadales	Sphingomonadaceae	Novosphingobium
Root154	Bacteria	Proteobacteria	Alphaproteobacteria	Sphingomonadales	Sphingomonadaceae	(unknown)
Root436	Bacteria	Proteobacteria	Alphaproteobacteria	Rhizobiales	Hyphomicrobiaceae	(unknown)
Root190	Bacteria	Actinobacteria	Actinobacteria	Actinomycetales	Nocardioidaceae	Nocardioides
Root265	Bacteria	Actinobacteria	Actinobacteria	Actinomycetales	Mycobacteriaceae	Mycobacterium
Root608	Bacteria	Proteobacteria	Alphaproteobacteria	Caulobacterales	Caulobacteraceae	Brevundimonas
Root708	Bacteria	Proteobacteria	Alphaproteobacteria	Rhizobiales	Rhizobiaceae	Rhizobium
Root404	Bacteria	Proteobacteria	Betaproteobacteria	Burkholderiales	Comamonadaceae	(unknown)
Root85	Bacteria	Actinobacteria	Actinobacteria	Actinomycetales	Intrasporangiaceae	(unknown)
Root1444	Bacteria	Proteobacteria	Betaproteobacteria	Burkholderiales	Comamonadaceae	(unknown)
Root720	Bacteria	Proteobacteria	Alphaproteobacteria	Sphingomonadales	Sphingomonadaceae	Sphingomonas
Root224	Bacteria	Actinobacteria	Actinobacteria	Actinomycetales	Nocardioidaceae	Nocardioides
Root670	Bacteria	Proteobacteria	Alphaproteobacteria	Rhizobiales	Methylobacteriaceae	(unknown)
Root685	Bacteria	Proteobacteria	Alphaproteobacteria	Rhizobiales	Hyphomicrobiaceae	(unknown)
Root63	Bacteria	Actinobacteria	Actinobacteria	Actinomycetales	Streptomycetaceae	Streptomyces
Root52	Bacteria	Firmicutes	Bacilli	Bacillales	Paenibacillaceae	Paenibacillus
Root405	Bacteria	Proteobacteria	Betaproteobacteria	Burkholderiales	Comamonadaceae	(unknown)
Root444D2	Bacteria	Firmicutes	Bacilli	Bacillales	Paenibacillaceae	Paenibacillus
Root494	Bacteria	Proteobacteria	Gammaproteobacteria	Xanthomonadales	Xanthomonadaceae	(unknown)
Root413D1	Bacteria	Proteobacteria	Alphaproteobacteria	Rhizobiales	Hyphomicrobiaceae	(unknown)
Root1280	Bacteria	Proteobacteria	Gammaproteobacteria	Pseudomonadales	Moraxellaceae	Acinetobacter
Root66D1	Bacteria	Actinobacteria	Actinobacteria	Actinomycetales	Streptomycetaceae	Streptomyces
Root101	Bacteria	Actinobacteria	Actinobacteria	Actinomycetales	Intrasporangiaceae	Janibacter
Root1310	Bacteria	Actinobacteria	Actinobacteria	Actinomycetales	Streptomycetaceae	Streptomyces
Root480	Bacteria	Proteobacteria	Gammaproteobacteria	Xanthomonadales	Xanthomonadaceae	(unknown)
Root170	Bacteria	Proteobacteria	Betaproteobacteria	Burkholderiales	Alcaligenaceae	Achromobacter
Root186	Bacteria	Bacteroidetes	Flavobacteriia	Flavobacteriales	Flavobacteriaceae	Flavobacterium
Root342	Bacteria	Proteobacteria	Alphaproteobacteria	Caulobacterales	Caulobacteraceae	Caulobacter
Root954	Bacteria	Proteobacteria	Alphaproteobacteria	Rhizobiales	Rhizobiaceae	Rhizobium
Root29	Bacteria	Proteobacteria	Betaproteobacteria	Burkholderiales	Comamonadaceae	(unknown)
Root690	Bacteria	Proteobacteria	Gammaproteobacteria	Xanthomonadales	Xanthomonadaceae	(unknown)
Root655	Bacteria	Proteobacteria	Alphaproteobacteria	Caulobacterales	Caulobacteraceae	Caulobacter
Root71	Bacteria	Proteobacteria	Gammaproteobacteria	Pseudomonadales	Pseudomonadaceae	Pseudomonas
Root332	Bacteria	Actinobacteria	Actinobacteria	Actinomycetales	Microbacteriaceae	(unknown)
Root236	Bacteria	Actinobacteria	Actinobacteria	Actinomycetales	Nocardioidaceae	Aeromicrobium
Root695	Bacteria	Proteobacteria	Alphaproteobacteria	Rhizobiales	Phyllobacteriaceae	Mesorhizobium
Root149	Bacteria	Proteobacteria	Alphaproteobacteria	Rhizobiales	Rhizobiaceae	Rhizobium
Root700	Bacteria	Proteobacteria	Alphaproteobacteria	Caulobacterales	Caulobacteraceae	(unknown)
Root81	Bacteria	Actinobacteria	Actinobacteria	Actinomycetales	Microbacteriaceae	Agromyces
Root241	Bacteria	Proteobacteria	Alphaproteobacteria	Sphingomonadales	Sphingomonadaceae	Sphingomonas
Root1257	Bacteria	Actinobacteria	Actinobacteria	Actinomycetales	Nocardioidaceae	Nocardioides
Root553	Bacteria	Actinobacteria	Actinobacteria	Actinomycetales	Microbacteriaceae	(unknown)
Root1237	Bacteria	Proteobacteria	Betaproteobacteria	Burkholderiales	Comamonadaceae	(unknown)
Root181	Bacteria	Actinobacteria	Actinobacteria	Actinomycetales	Intrasporangiaceae	(unknown)
Root1462	Bacteria	Proteobacteria	Alphaproteobacteria	Rhizobiales	Bradyrhizobiaceae	(unknown)
Root83	Bacteria	Proteobacteria	Betaproteobacteria	Burkholderiales	Alcaligenaceae	Achromobacter
Root239	Bacteria	Firmicutes	Bacilli	Bacillales	Bacillaceae	Bacillus
Root1485	Bacteria	Proteobacteria	Betaproteobacteria	Burkholderiales	Oxalobacteraceae	Massilia
Root135	Bacteria	Actinobacteria	Actinobacteria	Actinomycetales	Mycobacteriaceae	Mycobacterium
Root73	Bacteria	Proteobacteria	Alphaproteobacteria	Rhizobiales	Rhizobiaceae	Rhizobium
Root930	Bacteria	Actinobacteria	Actinobacteria	Actinomycetales	Cellulomonadaceae	(unknown)
Root131	Bacteria	Firmicutes	Bacilli	Bacillales	Bacillaceae	Bacillus
Root274	Bacteria	Proteobacteria	Alphaproteobacteria	Rhizobiales	Rhizobiaceae	(unknown)
Root418	Bacteria	Proteobacteria	Betaproteobacteria	Burkholderiales	Oxalobacteraceae	Janthinobacterium

Table S6: Genes in the pathways defined based on metabolic modeling (related to STAR Methods)

Pathway	Gene ID
Maltose	AT1G01090 // AT1G02640 // AT1G04410 // AT1G05610 // AT1G08480 // AT1G11720 // AT1G12900 // AT1G13440 // AT1G16300 // AT1G20860 // AT1G23190 // AT1G24180 // AT1G26560 // AT1G27680 // AT1G30120 // AT1G32380 // AT1G32440 // AT1G34430 // AT1G42970 // AT1G47420 // AT1G47840 // AT1G48030 // AT1G53240 // AT1G54220 // AT1G56190 // AT1G59900 // AT1G61800 // AT1G70730 // AT1G70820 // AT1G71750 // AT1G79530 // AT1G79550 // AT2G01140 // AT2G05710 // AT2G17130 // AT2G18450 // AT2G19860 // AT2G20420 // AT2G21170 // AT2G21330 // AT2G21770 // AT2G22480 // AT2G22780 // AT2G25540 // AT2G34590 // AT2G35390 // AT2G36390 // AT2G36460 // AT2G42910 // AT2G44350 // AT2G44450 // AT2G44480 // AT2G44530 // AT2G46390 // AT2G46505 // AT2G47510 // AT3G01180 // AT3G04050 // AT3G04120 // AT3G12780 // AT3G13930 // AT3G15020 // AT3G16950 // AT3G17240 // AT3G17940 // AT3G18080 // AT3G25960 // AT3G26650 // AT3G27380 // AT3G43190 // AT3G47000 // AT3G47050 // AT3G47520 // AT3G47800 // AT3G47833 // AT3G49160 // AT3G52200 // AT3G52930 // AT3G52990 // AT3G53900 // AT3G55410 // AT3G55440 // AT3G55650 // AT3G55810 // AT4G16155 // AT4G17090 // AT4G18240 // AT4G18780 // AT4G24620 // AT4G26270 // AT4G26390 // AT4G26520 // AT4G26530 // AT4G26910 // AT4G26970 // AT4G29130 // AT4G29220 // AT4G32210 // AT4G32410 // AT4G32840 // AT4G35830 // AT4G37840 // AT4G38970 // AT4G39210 // AT4G39350 // AT5G03650 // AT5G03690 // AT5G05170 // AT5G08300 // AT5G08570 // AT5G09600 // AT5G09660 // AT5G09870 // AT5G12860 // AT5G15140 // AT5G17420 // AT5G17520 // AT5G17630 // AT5G19220 // AT5G20830 // AT5G23250 // AT5G24300 // AT5G33320 // AT5G42260 // AT5G42740 // AT5G43330 // AT5G44030 // AT5G44640 // AT5G48300 // AT5G49190 // AT5G50850 // AT5G50950 // AT5G51820 // AT5G52920 // AT5G54800 // AT5G55070 // AT5G56350 // AT5G56630 // AT5G56720 // AT5G57655 // AT5G58330 // AT5G61580 // AT5G62575 // AT5G63680 // AT5G64740 // AT5G65685 // AT5G66570 // AT5G66760
Glucose	AT1G02640 // AT1G26560 // AT2G21770 // AT2G25540 // AT2G44450 // AT2G44480 // AT3G17940 // AT3G18080 // AT3G43190 // AT3G47000 // AT3G47050 // AT3G47800 // AT4G18780 // AT4G32410 // AT4G39350 // AT5G05170 // AT5G09870 // AT5G15140 // AT5G17420 // AT5G20830 // AT5G42260 // AT5G44030 // AT5G44640 // AT5G49190 // AT5G57655 // AT5G64740
beta-D-Fructose	AT1G01090 // AT1G04410 // AT1G08480 // AT1G12240 // AT1G21270 // AT1G23190 // AT1G24180 // AT1G27450 // AT1G30120 // AT1G32380 // AT1G34430 // AT1G47420 // AT1G47840 // AT1G47960 // AT1G48030 // AT1G53240 // AT1G54220 // AT1G59900 // AT1G61800 // AT1G62660 // AT1G70730 // AT1G70820 // AT1G71750 // AT1G80050 // AT2G05710 // AT2G17130 // AT2G18450 // AT2G19860 // AT2G20420 // AT2G22780 // AT2G34590 // AT2G35390 // AT2G36190 // AT2G42910 // AT2G44350 // AT2G44530 // AT2G46390 // AT2G46505 // AT2G47510 // AT3G13790 // AT3G13930 // AT3G15020 // AT3G16950 // AT3G17240 // AT3G27380 // AT3G47520 // AT3G47833 // AT3G52200 // AT3G55440 // AT3G61240 // AT4G16155 // AT4G22570 // AT4G23900 // AT4G24620 // AT4G26910 // AT4G26970 // AT4G29130 // AT4G32210 // AT4G35830 // AT4G37840 // AT5G08300 // AT5G09600 // AT5G09660 // AT5G09870 // AT5G11160 // AT5G12860 // AT5G17310 // AT5G17630 // AT5G20280 // AT5G23250 // AT5G23630 // AT5G42740 // AT5G43330 // AT5G50850 // AT5G50950 // AT5G51820 // AT5G54800 // AT5G55070 // AT5G56720 // AT5G58330 // AT5G62575 // AT5G63310 // AT5G64620 // AT5G65750 // AT5G66760
D-Galactose	AT1G12780 // AT1G23190 // AT1G30620 // AT1G47840 // AT1G63180 // AT1G64440 // AT1G70730 // AT1G70820 // AT2G19860 // AT2G34850 // AT3G06580 // AT3G10700 // AT3G43190 // AT4G23920 // AT4G29130 // AT4G37840 // AT5G17310 // AT5G18200 // AT5G20830 // AT5G49190 // AT5G51820 // AT5G57655
D-Xylose	AT1G02640 // AT1G06030 // AT1G12230 // AT1G26560 // AT1G47840 // AT1G63290 // AT1G66430 // AT1G71100 // AT2G01140 // AT2G01290 // AT2G19860 // AT2G21170 // AT2G21330 // AT2G22480 // AT2G31390 // AT2G36460 // AT2G44450 // AT2G44480 // AT2G45290 // AT3G01850 // AT3G04790 // AT3G17940 // AT3G18080 // AT3G43190 // AT3G47000 // AT3G47050 // AT3G47800 // AT3G52930 // AT3G55440 // AT3G59480 // AT3G60750 // AT4G10260 // AT4G26270 // AT4G26520 // AT4G26530 // AT4G29130 // AT4G29220 // AT4G32840 // AT4G37840 // AT4G38970 // AT5G03690 // AT5G13420 // AT5G15140 // AT5G16150 // AT5G20830 // AT5G42260 // AT5G44640 // AT5G49190 // AT5G49650 // AT5G51830 // AT5G56630 // AT5G57655 // AT5G61410 // AT5G61580
Glucose + beta-D-Fructose	AT1G12240 // AT1G21270 // AT1G47960 // AT1G62660 // AT5G64620
Glucose + D-Galactose	AT1G12780 // AT1G30620 // AT1G63180 // AT1G64440 // AT2G34850 // AT3G06580 // AT3G10700 // AT3G43190 // AT4G23920 // AT5G18200 // AT5G20830 // AT5G49190 // AT5G57655
Glucose + D-Xylose	AT1G02640 // AT1G12230 // AT1G26560 // AT1G63290 // AT1G71100 // AT2G01140 // AT2G01290 // AT2G21170 // AT2G21330 // AT2G21770 // AT2G22480 // AT2G25540 // AT2G36460 // AT2G44450 // AT2G44480 // AT2G45290 // AT3G01850 // AT3G04790 // AT3G17940 // AT3G18080 // AT3G43190 // AT3G47000 // AT3G47050 // AT3G47800 // AT3G52930 // AT3G55440 // AT3G60750 // AT4G18780 // AT4G26270 // AT4G26520 // AT4G26530 // AT4G29220 // AT4G32410 // AT4G32840 // AT4G38970 // AT4G39350 // AT5G03690 // AT5G05170 // AT5G09870 // AT5G13420 // AT5G15140 // AT5G17420 // AT5G20830 // AT5G42260 // AT5G44030 // AT5G44640 // AT5G49190 // AT5G49650 // AT5G56630 // AT5G57655 // AT5G61410 // AT5G61580 // AT5G64740
beta-D-Fructose + D-Galactose	AT1G06030 // AT1G12240 // AT1G12780 // AT1G21270 // AT1G23190 // AT1G30620 // AT1G47840 // AT1G47960 // AT1G62660 // AT1G63180 // AT1G64440 // AT1G66430 // AT1G70730 // AT1G70820 // AT2G19860 // AT2G31390 // AT2G34850 // AT3G06580 // AT3G10700 // AT3G59480 // AT4G10260 // AT4G23920 // AT4G24620 // AT4G29130 // AT4G37840 // AT5G17310 // AT5G18200 // AT5G42740 // AT5G51820 // AT5G51830 // AT5G57655 // AT5G64620
beta-D-Fructose + D-Xylose	AT1G01090 // AT1G04410 // AT1G06030 // AT1G08480 // AT1G09780 // AT1G12230 // AT1G12240 // AT1G12900 // AT1G13440 // AT1G16300 // AT1G16350 // AT1G21270 // AT1G23190 // AT1G24180 // AT1G30120 // AT1G32380 // AT1G32440 // AT1G34430 // AT1G42970 // AT1G47420 // AT1G47840 // AT1G47960 // AT1G48030 // AT1G53240 // AT1G54220 // AT1G56190 // AT1G59900 // AT1G62660 // AT1G63290 // AT1G66430 // AT1G70730 // AT1G70820 // AT1G71100 // AT1G71750 // AT1G74030 // AT1G79470 // AT1G79530 // AT1G79550 // AT2G01140 // AT2G01290 // AT2G05710 // AT2G17130 // AT2G18450 // AT2G19860 // AT2G20420 // AT2G21170 // AT2G21330 // AT2G22480 // AT2G22780 // AT2G31390 // AT2G34590 // AT2G35390 // AT2G36460 // AT2G36530 // AT2G42910 // AT2G44350 // AT2G44530 // AT2G45290 // AT2G46390 // AT2G46505 // AT2G47510 // AT3G01850 // AT3G04050 // AT3G04120 // AT3G04790 // AT3G08590 // AT3G12780 // AT3G13930 // AT3G15020 // AT3G16950 // AT3G17240 // AT3G25960 // AT3G26650 // AT3G27380 // AT3G43190 // AT3G47520 // AT3G47833 // AT3G49160 // AT3G50520 // AT3G52200 // AT3G52930 // AT3G52990 // AT3G55410 // AT3G55440 // AT3G55650 // AT3G55810 // AT3G59480 // AT3G60750 // AT4G10260 // AT4G16155 // AT4G23900 // AT4G26270 // AT4G26390 // AT4G26520 // AT4G26530 // AT4G26910 // AT4G26970 // AT4G29130 // AT4G29220 // AT4G32210 // AT4G32840 // AT4G35830 // AT4G37840 // AT4G38970 // AT5G03690 // AT5G08300 // AT5G08570 // AT5G09600 // AT5G09660 // AT5G09870 // AT5G12860 // AT5G13420 // AT5G17310 // AT5G20830 // AT5G23250 // AT5G43330 // AT5G47840 // AT5G49190 // AT5G49650 // AT5G50370 // AT5G50850 // AT5G50950 // AT5G51820 // AT5G51830 // AT5G52920 // AT5G55070 // AT5G56350 // AT5G56630 // AT5G56720 // AT5G57655 // AT5G58330 // AT5G61410 // AT5G61580 // AT5G62575 // AT5G63310 // AT5G63680 // AT5G64620 // AT5G65750 // AT5G66760
D-Galactose + D-Xylose	AT1G06030 // AT1G12230 // AT1G12240 // AT1G12780 // AT1G21270 // AT1G23190 // AT1G30620 // AT1G47840 // AT1G47960 // AT1G62660 // AT1G63180 // AT1G63290 // AT1G66430 // AT1G66430 // AT1G70730 // AT1G70820 // AT1G71100 // AT2G01140 // AT2G01290 // AT2G21170 // AT2G21330 // AT2G22480 // AT2G23190 // AT2G34850 // AT2G36460 // AT2G45290 // AT3G01850 // AT3G04790 // AT3G17940 // AT3G18080 // AT3G10700 // AT3G52930 // AT3G55440 // AT3G59480 // AT3G60750 // AT4G10260 // AT4G23920 // AT4G24620 // AT4G26270 // AT4G26520 // AT4G26530 // AT4G29130 // AT4G29220 // AT4G32840 // AT4G37840 // AT4G38970 // AT5G03690 // AT5G13420 // AT5G17310 // AT5G18200 // AT5G42740 // AT5G49650 // AT5G51820 // AT5G51830 // AT5G56630 // AT5G57655 // AT5G61410 // AT5G61580 // AT5G64620
SWEET1	AT1G21460
SWEET2	AT3G14770
SWEET3	AT5G53190
SWEET4	AT3G28007
SWEET5	AT5G62850
SWEET6	AT1G66770
SWEET7	AT4G10850
SWEET8	AT5G40260
SWEET9	AT2G39060
SWEET10	AT5G50790
SWEET11	AT3G48740
SWEET12	AT5G23660
SWEET13	AT5G50800
SWEET14	AT4G25010
SWEET15	AT5G13170
SWEET16	AT3G16690
SWEET17	AT4G15920
SUC1	AT1G71880
SUC2	AT1G22710
SUC3	AT2G02860
SUC4	AT1G09960
SUC5	AT1G71890
SUC6	AT5G43610
SUC7	AT1G66570
SUC8	AT2G14670
SUC9	AT5G06170



Data S1: Contribution of each metabolite to the two principle components that explain the largest variation (PC1 and PC2) of PCA for each plant genotype (related to Figure 4)